

1

NOvA Test Beam detector calibration

2

Technical Note

3

Robert Kralik

University of Sussex

4

September 13, 2023

5

Abstract

6

What is this about and what will I describe in here

7

Contents

8	1	Introduction	2
9	2	Overview of the Test Beam detector	4
10	3	NOvA calibration process	7
11	3.1	Relative calibration	12
12	3.2	Absolute calibration	13
13	3.3	Calibration uncertainties	13
14	4	NOvA Test Beam detector calibration	13
15	4.1	Overview	13
16	4.1.1	Definitions	14
17	4.2	Fiber Brightness	14
18	4.3	Simulation	14
19	4.4	Threshold and shielding corrections	16
20	4.5	Period 1	16
21	4.6	Period 2	17
22	4.6.1	Relative calibration results	17
23	4.7	Period 3	17
24	4.7.1	Relative calibration results	23
25	4.8	Period 4	23
26	4.8.1	Relative calibration results	23
27	4.9	Absolute calibration results	23
28	4.10	Drift in TB data	26
29	4.11	Results	26
30	4.12	Validation	26

31 1 Introduction

32 TO DO:

- 33 • Divide the motivation to abstract (why do we care about test beam calibration, what did
34 we do and how did we do it. What are the results)
- 35 • and introduction (brief history of test beam calibration, maybe a bit more detail into why
36 is test beam calibration important)

37 Why is Test Beam? "The idea, as with any test beam experiment, is to expose a detector
38 to a beam of very well-characterized particles, so that we can improve our understanding our
39 how the detector responds to such particles. We make use of upstream detectors to collect
40 data on the beam particles before they interact in the NOvA detector. For example, we will
41 be able to see what a 1 GeV proton actually looks like in our detector, without having to
42 simulate it, and we can test how well we would have reconstructed the energy using our existing
43 techniques. We may find we are able to make improvements to our tools to better match what
44 we see in the detector with how we reconstruct it. Or we may find we already do a pretty
45 good job. Either way, with a full cross-comparison like this, we can be more confident in our
46 analysis of the data and reduce the level of uncertainty we consider are associated with the
47 relevant measured quantities. Ultimately, the aim will be to reduce the level of uncertainty on
48 the neutrino oscillation analyses and to make even better, more accurate measurements of the
49 Standard Model."Why is Test Beam calibration done:

- 50 • To be able to directly compare TB to the standard detectors
- 51 • To be able to verify our calibration procedures using TB data
- 52 • To study the particle response as a function of energy
- 53 • To determine an energy resolution
- 54 • To compare currently used energy scales to data and understand if we can use TB data
55 for absolute energy scale in all NOvA detectors

56 For DeltaM2: By increasing exposure, total syst. error decreases by (+) 18.5For sin2Th23:
57 Difference by reducing calib syst.: (+) 10.8Statement: "The NOvA Test Beam will improve
58 the total systema6c error on the final measurement of the oscillation parameters Dm232 and
59 sin2Th23 by 10Potential Test Beam impacts: Check modeling of hadronic interactions in de-
60 tector (check GEANT systemaOcs), Using Test Beam data as "single-particle MC" to train
61 CVN prong-like algorithms, Generative Adversarial Networks for MC improvements using
62 Test Beam data, Check ND calibraOon procedure to try and understand causes of 3-5

- 63 • Hadronic response and comparison with MC modeling
 - 64 – response as a function of energy
 - 65 – establishing of an absolute energy scale
 - 66 – determination of energy resolution
 - 67 – studies of topological features and resolution

- 68 * pion tracking and showers
69 * proton tracking and showers
70 – studies of timing features and resolution
71 • Electromagnetic response and comparison with MC modeling
72 – response as a function of energy
73 – establishing of an absolute energy scale
74 – determination of energy resolution
75 – studies of topological features and resolution
76 * electron signatures
77 * gamma signatures
78 – studies of timing features and resolution
79 – studies of π^0 from π^- charge-exchange
80 • Muon response and comparison with MC modeling
81 – comparison with detailed optical simulations
82 – determination of energy resolution
83 – studies of topological features and resolution
84 – cross-talk studies
85 – comparison to cosmic ray muons (requires a special trigger)
86 – studies of the muon calibration protocol
87 • Light yield and response studies as a function of particle type and detector configuration
88 – understanding the Cherenkov light contribution
89 – vertical and horizontal responses and comparison with simulations
90 – data with selected planes rotated by 45 and 90 degrees
91 – slanted (angle) plane response (and subset of programs as above)
92 – fiber attenuation studies
93 – Birks' constant studies
94 • Near / Far readout comparison
95 • Gather large libraries of particles at known energies and multiple angles of incidence to
96 help develop a CNN prong ID. Also allows training of a particle-based CVN-like PID.

97 Also use information from:

- 98 • NOvA Test Beam Technical Statement of Work
99 • NOvA Test Beam program (paper for DOE) [docdb:25074]

- 100 • NOvA Test Beam task force report [docdb:15750]
 101 • Overview presentation of NOvA Test Beam [docdb:20495]
 102 • Test Beam support document [docdb:22172]
 103 • NOvA Test Beam program proceedings [docdb:55808]
 104 Mike's proceedings from ICHEP 2020 [1].

105 2 Overview of the Test Beam detector

106 The NOvA Test Beam detector is a scaled down version of the Near and Far Detectors shown
 107 on figure 1. It is placed in the MC7b enclosure of the Fermilab Test Beam Facility in the path
 108 of the MCcenter beamline with a variety of beamline detectors to measure and identify a range
 109 of particles with various momenta [2].

110 Maybe also mention the specific times Test Beam detector was operational.

111 Majority of the Test Beam detector and it's instrumentation is identical to the other NOvA
 112 detectors, but there are a few differences, including size, scintillator oil used, readout electron-
 113 ics, or environmental controls, that we're discussing in this section.

114 Should I aslo talk about the beam halo? Could that have an influence on the calibration?

115 Maybe it's the peaks in the cosz distribution?

116 General parameters

117 The NOvA Test Beam detector consists of two 31-plane blocks, each beginning and ending
 118 with a vertical plane, with an additional horizontal plane glued inbetween them to preserve the
 119 alternating arrangement [3]. Each plane consists of 2 modules side-by-side and each module is
 120 made up of 32 cells. Each cell has an inner (without the PVC) depth and width of 5.9 cm and
 121 3.8 cm respectively, same as for the other NOvA detectors, and a length of 2.6 m. This brings
 122 the final dimensions of the Test Beam detector to 63 planes \times 64 cells, or $2.6 \times 2.6 \times 4.1 \text{ m}^3$.

123 The 63 planes are numbered from 0 to 62, with even numbers corresponding to vertical
 124 planes and odd numbers to horizontal planes. Cells are numbered 0 to 63, going from bottom
 125 to top for horizontal planes and left to right, when facing the front of the detector, for vertical
 126 planes.

127 The detector coordinate system is illustrated on figure 1. It is centered with $(0, 0, 0)$ in the
 128 centre of the first plane [4]. The x axis runs left to right when facing the front of the detector,
 129 y axis bottom to top, and z axis goes along the beam direction from front to the back of the
 130 detector. The exact geometry of the Test Beam detector from several alignment surveys is saved
 131 in gdml files and used in our analyses [5].

132 In the past we encountered an issue when aligning the Test Beam detector with the beamline
 133 measurements broke several assumptions within the Test Beam geometry [4], which manifested
 134 as uncalibrated cells in the back of the detector [6]. This was fixed by realigning both the
 135 detector and the beamline based on the last alignment survey and implemented in the production
 136 tag R23-04-05-testbeam-production.a and there after [4].

137 Should I define w here? And tehn mention it in the readout section to say that readout is
 138 always on the positive side of the detector. Additionally we use the coordinates measured by

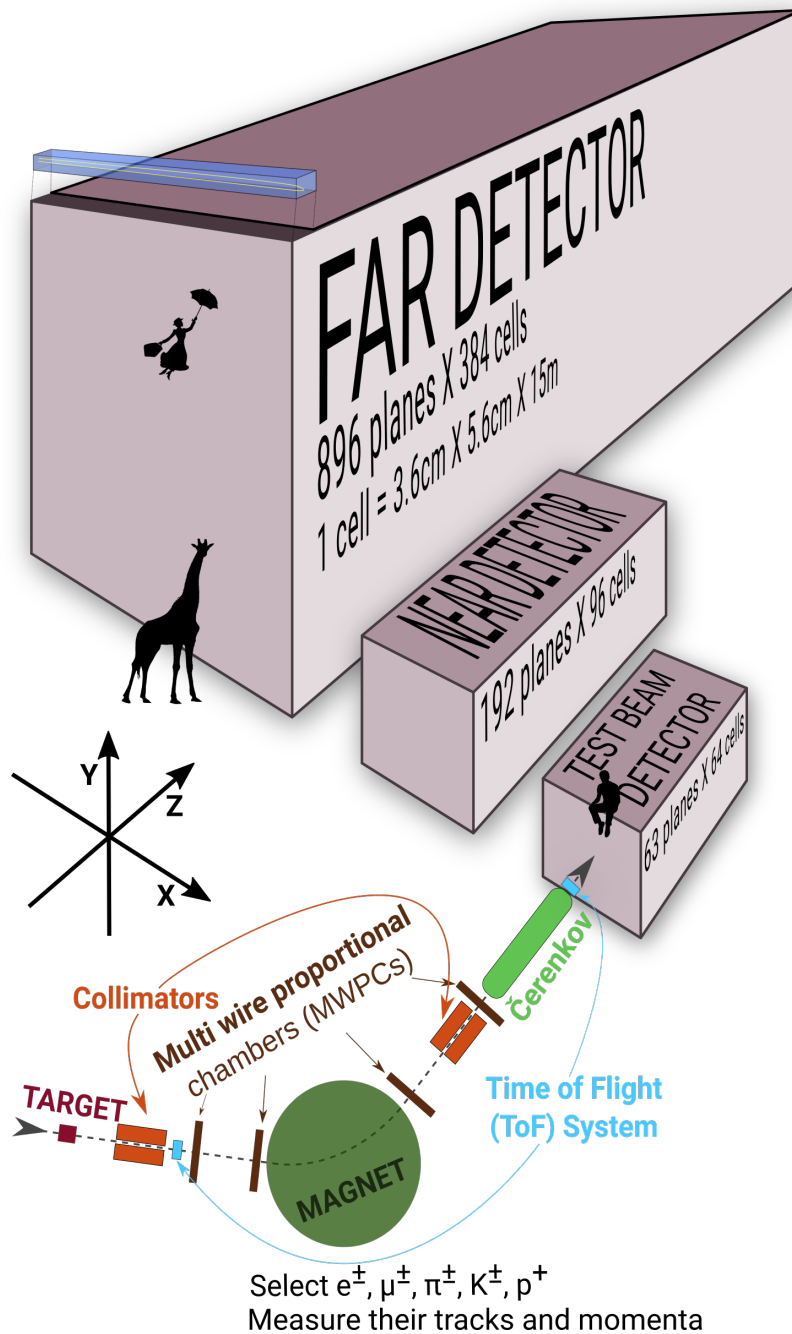


Figure 1: Comparison of Test Beam detector scale to the Near and Far NOvA detectors (and a man, giraffe, or Mary Poppins). Also shown are the Test Beam beamline detectors and components (not to scale), with arrows showing the direction of the beam. The three black arrows show the orientation fo the detector coordinate system.

- ¹³⁹ cell number V and the distance along the cell length W independent of the view in question.
- ¹⁴⁰ Extensive use of W is made throughout this document and the code. Note: W is not the distance
- ¹⁴¹ to the readout, it is simply an alias for x or y, so W = 0 is at the cente of detector. It happens that
- ¹⁴² the readout and coordinate system are arranged such that more positive values of W are closer
- ¹⁴³ to the readout. [docdb:13579 - SA The Attenuation and Threshold Calibration of the NOvA

144 detector]

145 Scintillator

146 The Test Beam detector is filled with (more than) three different versions of the NOvA scin-
147 tillator, which differ mainly in the way they were stored since the filling of the near and far
148 detectors. This is illustrated on figure 2.

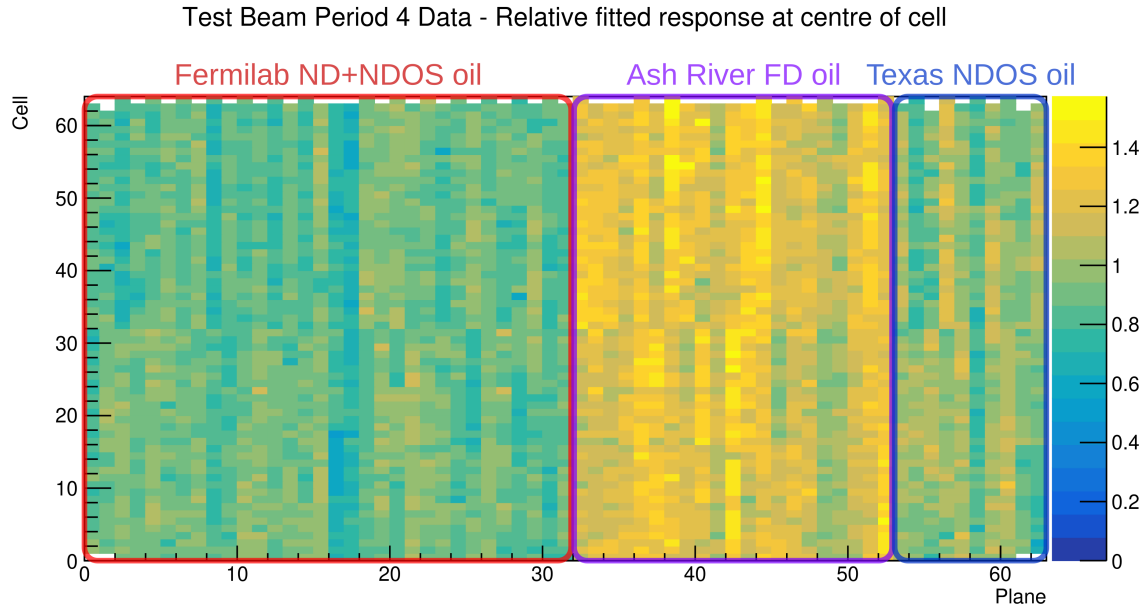


Figure 2: Uncorrected energy response in the centre of cells across the Test Beam detector showing a clear distinction between the different scintillator oils.

149 The original plan [7] was to use the scintillator from a tanker and one of the tanks located
150 outside in Fermilab. First tests showed acceptable results and the tanker oil was used to fill out
151 almost the entirety of the first block of the detector (first 32 planes) [8]. However, when we
152 loaded the oil from tank two into the tanker, it became extremely cloudy and unusable, possibly
153 due to contamination with water accumulated at the bottom of the tanks, which was mixed with
154 oil by the pump. The rest of the first block was topped up with high quality scintillator
155 from NDOS, which has been stored inside in barrels at MiniBooNE [9]. This is labeled as
156 "Fermilab ND+NDOS oil" on figure 2.

157 Even before the extreme cloudiness was discovered, it was known that the oil from the tanks
158 has lost much of its original light yield properties. Reasons vary from water contamination to
159 insects and dirt contamination [10]. Yet it was still decided to use the tank 2 oil [7]. It was
160 also decided not to mix the various oils (tanker/tank/NDOS/Ash River) as studying energy
161 deposition in different types of oils could lead to some interesting insights [10].

162 The first 21 planes of the second block (planes 32 to 52) were filled with the Far Detector
163 production scintillator shipped in from Ash River [11]. This oil has been stored in "totes"
164 inside a building and under several layers of black plastic [12]. Also used a little (70 gallons)
165 scintillator from NDOS to fill these planes (compared to 1900 gallons from Ash River) [11].

166 The last 10 planes (planes 53 to 62) [11] were filled with scintillator drained from NDOS
167 stored in Texas A&M University and University of Texas at Austin [13, 14]. This scintillator

168 has higher light yield than the one from the tanker, but lower than the Ash River one [13].

169 In total the Test Beam detector is filled with 5418 gallons of scintillator oil with a weight
170 of approximately 28.6 tons [3].

171 **Readout**

172 The Test Beam detector uses in total 126 front end boards (FEBs), each reading out signal from
173 32 cells (half of a plane) [3]. The readout is located on the top and right (looking on the front)
174 side of the detector. 118 FEBs are version 4.1, same as in the Far Detector, and 8 FEBs, located
175 on planes 16, 17, 48 and 49, are version 5.2, same as in the Near Detector. The Near Detector
176 FEBs are designed to read out data in a faster rate and we used a mix of FEB types to study the
177 difference in their response and to validate both versions in the same environment [15].

178 **Environment**

179 Unlike the near and the far detector, the Test Beam detector does not have any overburden to
180 shield it from cosmic particles.

181 Temperature very stable during winter months (heCng is installed at MC7). However, dew
182 point went over 10C ND shutdown threshold several times.

183 **Underfilled cells issue**

184 The Test Beam detector is slightly tilted around the Z axis by about 0.7° towards the readout.
185 This caused the top cells of both modules of all the horizontal planes (cells 31 and 63) to be
186 underfilled, creating an air bubble on the left side of the detector and severely affecting the
187 energy response in those cells [15]. This has been fixed [16] by adding extensions to the filling
188 ports and overfilling the horizontal cells with the NDOS scintillator stored in drums Fermilab
189 (not the scintillator store in a tanker or tanks). This scintillator was also used in the first half
190 of the detector (Fermilab ND+NDOS oil on figure 2), but is different from the "Ash River oil"
191 used in part of the second half of the detector (bright part of figure 2). The overfilling was done
192 in April 2021 in 3 stages in between the full operation of the Test Beam detector.

193 **3 NOvA calibration process**

194 Test Beam is following the same ideas and procedures as the standard NOvA calibration. This
195 section intends to provide only a brief overview of the NOvA calibration. Further details can
196 be found in the other NOvA calibration technical notes [17].

197 The purpose of calibration is to make sure that we get the same amount of energy wherever
198 or whenever it's deposited in whichever of NOvA's detectors and to express this energy in phys-
199 ical units. The NOvA calibration uses cosmic ray muons, which provide a consistent, abundant
200 and well-understood source of energy deposition and consists of two closely connected parts
201 [18]:

- 202 1. The **relative calibration** corrects for attenuation of scintillator light as it travels through
203 the cell to the readout, as well as for differences between detector cells.

204 2. This is followed by the **absolute calibration**, which only uses stopping muons when they
 205 are minimum ionising particles and calculates a scale between the measured charge read-
 206 out, corrected by the relative calibration, and the simulated energy deposition in physical
 207 units of MeV. This scale is calculated for each time period and each detector separately,
 208 which ensures the energy deposition is directly comparable wherever or whenever it oc-
 209 curred.

210 There is also **timing calibration**, which corrects for the time differences of the signal to be
 211 processed and is done as a separate project to the relative and absolute calibrations and is out
 212 of scope of this technical note [19].

213 The units and variables used to define energy deposited in NOvA detectors are listed in
 table 1:

ADC	The digitized charge collected by the APDs from the Analog to Digital Converter [20].
PE	Number of Photo Electrons. Calculated by a simple rescaling of the best estimate of the peak ADC. The PE per ADC scale only depends on the FEB type and the APD gain settings. This is technically done before the calibration and serves as the base unit for calibration.
PECorr	Corrected PE after applying the relative calibration results. The correction is a ratio between an average energy response (a pre-determined semi-arbitrary number) and the result of the the relative calibration fit (also called attenuation fit), which depends on w, cell, plane, epoch and detector. This makes the energy response equivalent across each detector.
MEU	Muon Energy Unit is the mean detector response to a stopping cosmic minimum ionising muon. Mean MeV/cm or mean PECorr/cm
MeV	Estimated energy deposited in the scintillator calculated from PECorr using the results of the absolute calibration. Additional correction for dead material needs to be made in order to get a calorimetric energy estimate.

Table 1: Definitions of variables commonly used in calibration [17, 18].

214 The final result of the NOvA calibration is the deposited energy in terms of physical units,
 which is in effect calculated as:

$$E_{dep}[\text{MeV}] = \underbrace{\frac{\text{MEU}_{truth}[\text{MeV}/\text{cm}]}{\text{MEU}_{reco}[\text{PECorr}/\text{cm}]}}_{\substack{\text{Absolute calibration} \\ (\text{Detector, epoch})}} \times \underbrace{\frac{\text{Average response}[\text{PECorr}]}{\text{Fitted response}[\text{PE}]}}_{\substack{\text{Relative calibration} \\ (\text{Detector, epoch,} \\ \text{plane, cell, w})}} \times \underbrace{\left[\frac{\text{PE}}{\text{ADC}} \right]}_{\substack{\text{Scale} \\ (\text{APD Gain, FEB})}} \times \text{Signal}[\text{ADC}], \quad (1)$$

215 where both the relative calibration results (blue fraction) and the absolute calibration results
 216 (red fraction) are stored in a database and applied together with the ADC-to-PE scale by the
 217 NOvASoft *Calibrator* package during processing of every hit in the NOvA detectors.

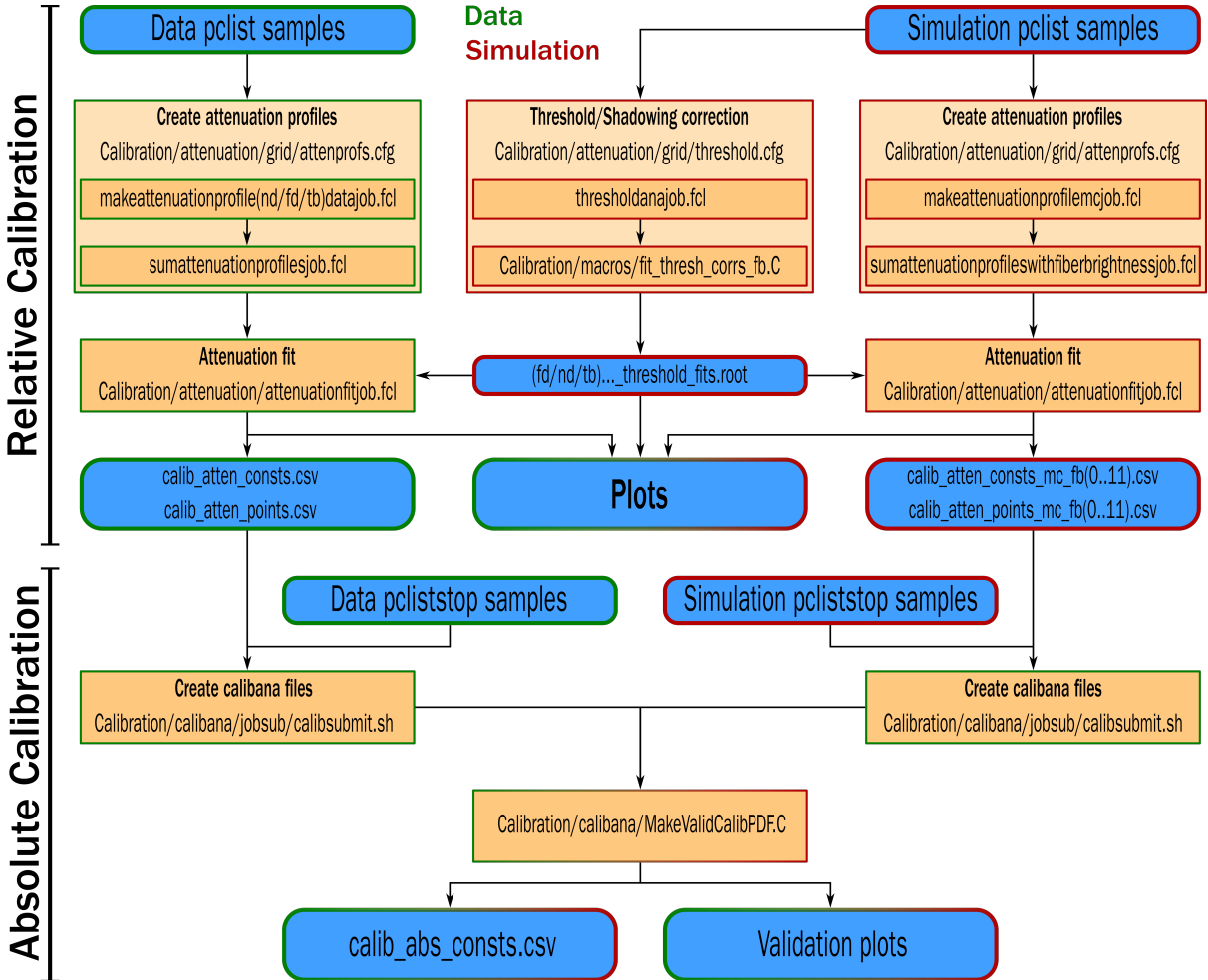


Figure 3: Flow chart showing the jobs (orange background) and files (blue background) needed and produced during the full NOvA calibration process. The left chain is showing the data calibration process (with green border) and is applied to every data calibration sample separately (periods or epochs). The center and right chains are showing the simulation calibration proces (red border), which is redone only if there's a change to the detector simulation. The absolute calibration at the bottom combines data and simulation. The entire process is done separately for each NOvA detector.

218 **Creating calibration samples**

219 To select good quality cosmic ray muons we first remove beam related events based on their
 220 time stamp relative to the time of the beam spill, as shown on figure 4. Then we apply basic
 221 reconstruction and track-based selection.

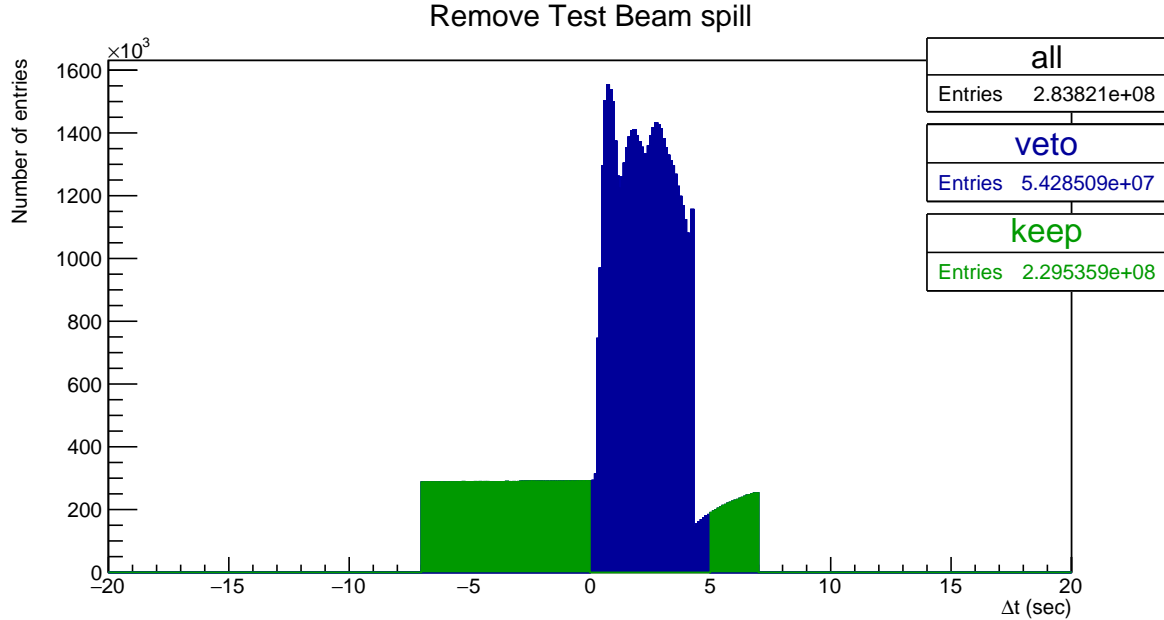


Figure 4: Test Beam beam spill events removed from the calibration samples. Test Beam beam spill is 4.2 seconds long and we remove events (in blue) within a 5 seconds window from the start of the beam spill. The remaining events (green) should mostly consist of cosmic particles. This example and the numbers of entries are for the full period 4 Test Beam sample.

222 Since energy deposition in a cell depends on the pathlength the particle traveled through
 223 the cell, we only use hits for which we can reliably calculate their pathlength. We call these
 224 hits **tricell** hits, as we require that all accepted hits also have a recorded hit in both neighboring
 225 cells of the same plane, as shown on figure 5. In case there's a bad channel in a neighboring
 226 cell, we ignore this channel and look one cell further. We can then calculate the pathlength
 227 simply as the cell width divided by the cosine of the direction angle [17, 18].

228 For the absolute calibration we select muons that stop in the detector. For this we identify
 229 muons with a Michel electron at the end of their track and only selection those [21].

230 For each data period/epoch and each simulation version we create two calibration samples
 231 that are used as the input for the relative and absolute calibration. The samples are called [22]

- 232 • pclist = **list** of **pre-calibrated hist**; Contains all selected cosmic muon events and is used
 233 in the relative calibration;
- 234 • pcliststop = pclist files only containing stopping muons used for the absolute calibration

235 **Fiber brightness**

236 For data, the relative calibration is done for each individual cell in each plane to properly
 237 account for any potential variations. Therefore we have to repeat the attenuation fit $N_{cell} \times$

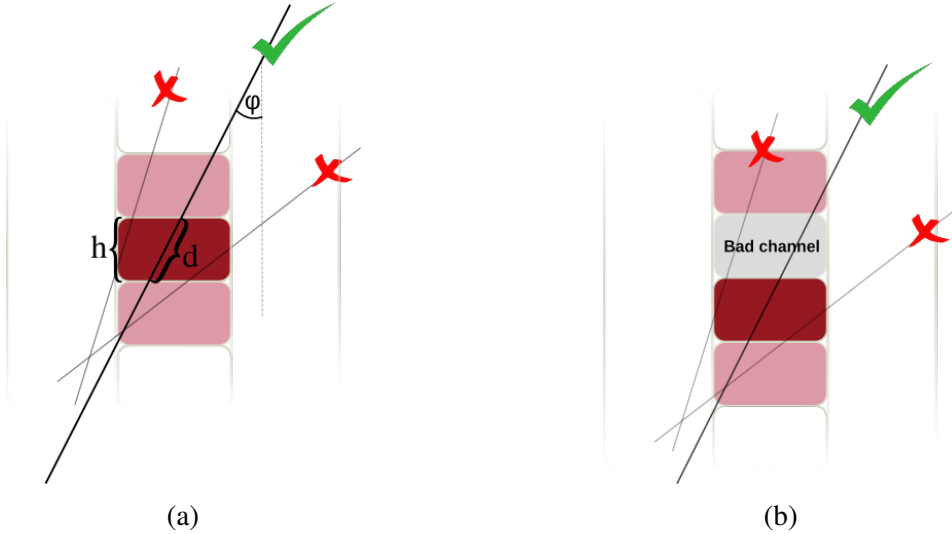


Figure 5: Illustration of the tricell condition (a). We only use hits that have two surrounding hits in the same plane to be used in the NOvA calibration. This is to ensure a good quality of the pathlength (d) reconstruction, which is calculated from the known cell height (h) and the reconstructed track angle (ϕ). In case the hit is next to a bad channel (b), we ignore this bad channel and require a hit in the next cell over.

238 N_{plane} times. However, generating enough simulated events would be very computationally
239 intensive. Additionally, we can assume that the simulated detector is approximately uniform
240 plane to plane. Therefore, for simulation, we want to *consolidate* the detector planes and only
241 consider variation in the two views and their cells, so repeat the fit $N_{cell} \times N_{view}$ times [23, 24].

242 There are some variations in the detector response cell by cell, that can be caused by different
243 fiber brightnesses, but also by different qualities of the scintillator, air bubbles, APD gains,
244 looped or zipped fibers and potentially others. To emulate these differences in the simulation
245 without the need to simulate every cell individually and properly, we divide all the cells of
246 each detector into 12 brightness bins, as shown on figure 6. These bins describe the relative
247 differences in the detector response between individual cells [24]. Therefore in the end, for
248 simulation we perform the attenuation fit in the $N_{view} \times N_{fiberbrightnessbin} \times N_{cell}$ phase space.

249 Threshold and shielding correction

250 Energy deposited far away from the readout may get attenuated enough to be shifted below
251 the threshold. These low energy depositions would be mising from the attenuation fit, biasing
252 it towards larger light levels going away from the readout. A similar effect, specifically for
253 the vertical cells, is caused by using cosmic muons for calibration. The top of the detector ef-
254 ffectively shields the bottom of the detector, skewing the energy distribution of cosmic muons.
255 To correct for both of these effect, we use simulation to calculate the threshold and shield-
256 ing (also called threshold and shadowing) correction by comparing the true and reconstructed
257 information. We apply this correction before the attenuation fits [23].

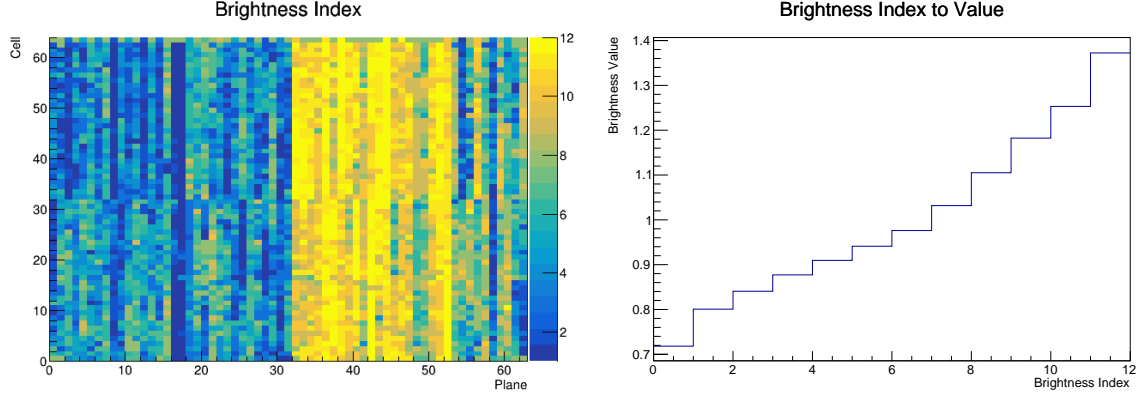


Figure 6: The Test Beam detector is (like the standard NOvA detectors) divided into 12 brightness bins (left plot), each representing a relative difference in energy response (right plot) due to different brightnesses of the fibers, scintillators, or readout.

258 3.1 Relative calibration

259 Relative calibration aims to create a fit, called *attenuation fit*, to the detector response over the
 260 position in a cell separately for every cell inside each detector. Scaling the fitted response to
 261 match the "average response" of the detector effectively removes relative differences through-
 262 out and between all cells across the entire detector. This average response is a single number
 263 chosen to approximately represent the average response in the middle of the cell. For the Far
 264 Detector this number is 39.91 PE, for the Near Detector it's 37.51 and for Test Beam it's the
 265 same as for the Far Detector 39.91. The scale of this number has no impact of this result as the
 266 absolute scale of the detector response is determined during the absolute calibration [18, 23].

267 To create the attenuation fit we follow the following procedure [18]:

- 268 1. Create *attenuation profiles*, which are profile histograms of detector response in terms of
 269 energy deposited per pathlength (PE/cm) as a function of position in the cell (w) through
 270 each cell for all planes. We construct the attenuation profiles over a little wider range
 271 than the actual length of the cell and always with 100 bins for each detector. This means
 272 that smaller detectors, like the Test Beam detector, have a finer binning ($\sim 3\text{cm/bin}$)
 273 compared to the Far Detector ($\sim 18\text{cm/bin}$).
- 274 2. Analyse the attenuation profiles. The job to create the attenuation profiles also creates
 275 validation histograms, which should be analyzed prior to performing the attenuation fit
 276 to make sure the attenuation profiles look as expected.
- 277 3. Apply the threshold and shielding correction that were created using the simulation plist
 278 sample before the relative calibration.
- 279 4. Do the attenuation fit over the full length of each cell. The fit consists of
 - (a) exponential fit, which combines two cases. Light from the energy deposition traveling straight to the readout, or going the opposite direction, looping around the cell and then to the readout. The fitted function has a form:

$$y = C + A \left(\exp\left(\frac{w}{X}\right) + \exp\left(-\frac{L+w}{X}\right) \right), \quad (2)$$

280 where y is the response, L is the length of the cell and C , A and X are the fitted
281 parameters. X also represents the attenuation length.

- 282 (b) To remove the effect of residuals, mainly at the end of cells, we smooth out the
283 residuals from the exponential fit with LOcally WEighted Scatter plot Smoothing
284 (LOWESS).

285 5. Check the plots of the attenuation fit for a selection of cells.

286 6. Save the fit result to the database in the form of two csv tables. The *calib_atten_consts.csv*
287 table holds the results of the exponential fit, together with the final χ^2 of the fit. The
288 *calib_atten_points.csv* table holds the results of the LOWESS smoothing.

289 To ensure the quality of the attenuation fit, we only apply the results if the final $\chi^2 < 0.2$.

290 If $\chi^2 > 0.2$ we ignore the results for this cell and mark it as *uncalibrated*.

291 3.2 Absolute calibration

292 To find the absolute energy scale, we apply the relative calibration results on the stopping muon
293 sample and look at the energy they deposited in cells 1-2 meters from the end of their tracks.
294 In this track window they are minimum ionising particles and their energy deposition is almost
295 constant and well understood. We take a mean of their corrected deposited energy separate for
296 each view and for each calibrated sample. We then take the average over the two views to get
297 the final MEU_{reco}PECorr/cm for each sample [21].

298 From simulation we get the mean of the true energy deposited in scintillator MEU_{truth}MeV/cm
299 for the same sample of stopping muons. We ignore the energy that's lost in the dead material
300 (PVC extrusions) and deal with it separately. The absolute energy scale for each sample is then
301 the ratio of MEU_{truth}/MEU_{reco}. We save these absolute energy scales in another csv table called
302 *calib_abs_consts.csv* which stores the MEU values and their errors.

303 As part of the absolute calibration we also produce validation plots that show the effect of
304 calibration on the distribution of the stopping muons. We analyse these plots and if everything
305 looks all right load all the csv tables into the database.

306 3.3 Calibration uncertainties

307 WORK IN PROGRESS

308 4 NOvA Test Beam detector calibration

309 4.1 Overview

310 History of TB calibration. What led to the final version of TB calibration. What can be done
311 next. I think this could also be in the introduction?

312 Dates and times when the data taking occurred.

313 Adding the underfilled cells to the bad channels which are automatically skipped for the
314 tricell condition

315 Period naming, possibly epochs (for P3). List of data samples, plus MC samples that were
316 used and pointer to the data-based simulation technote.

317 Specific running conditions: - maybe enough to mention this in the individual descriptions
318 of the test beam periods Underfilled cells Faulty FEBs (Period 2 and Period 3)

319 Why do we do the calibration generally and why do we need to do in for Test Beam specific-
320 ically - probably in the introduction

321 Temperature study (small overview)

322 From Teresa's thesis Along with setting the energy scale of the detector, we need to calibrate
323 the timing of the readout system for the detector. The Data Concentrator Modules (DCMs)
324 responsible for collating the data from multiple FEBs get their timing information via a daisy
325 chain originating at the detector TDU. Each DCM in the chain has a timing offset relative to the
326 DCM before it, with the last DCM having the earliest ti. Following the procedure described in
327 [66], I used timing information from hits on cosmic ray muon tracks that pass through multiple
328 DCMs to determine the relative offsets between DCMs, shown in Figure 3.20.

329 4.1.1 Definitions

330 List all final data and simulation definitions used.

331 Mention exactly the name and the location of the fcl files to create the TB plist/peliststop
332 files.

333 When were these files produced? Mention that we had to reprocess most of the files in 2023
334 due to the changed geometry.

335 From Teresa's thesis: "For Test Beam, we have three beam-based triggers, one pulsed trig-
336 ger, and two data-driven triggers. The data-driven triggers are both activity-based triggers. The
337 first is intended to record cosmic ray induced events for use in calibrating the detector.

338 4.2 Fiber Brightness

339 To divide the Test Beam detector into fiber brightness bins we used the attenuation fit results
340 for period 4 data (described in section 4.8).

341 Describe and show plots that since we are only using the fitted response at cell centre we
342 can allow fits with $\chi^2 > 0.2$. Show examples of responses with chisq larger than that and say
343 what is the final chisq chosen. No need to show the final distribution of the fb bins here as they
344 were technically shown in the general calibration description. But might refer back to it...

345 4.3 Simulation

346 We originally used Teresa's calibration MC sample, but after we saw disagreement, we devel-
347 oped a new MC based off of the period 3 data, which we ended up using for both period 2 and
348 period 3. For fibre brightness we are also using the same MC from period 3 data as it represents
349 the detector in its best condition.

350 We used a data-based simulation of cosmic muons for the Test Beam detector calibration.
351 The details are described in the technote XXX. We used this and this data as a basis and this
352 and this data for the fiber brightness file.

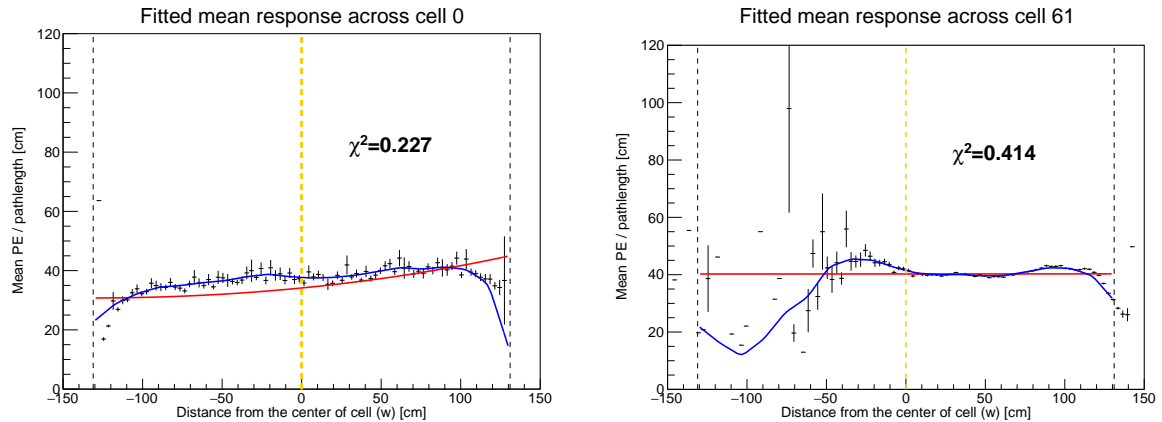


Figure 7: The Test Beam detector is (like the standard NOvA detectors) divided into 12 brightness bins (left plot), each representing a relative difference in energy response (right plot) due to different brightnesses of the fibers, scintillators, or readout.

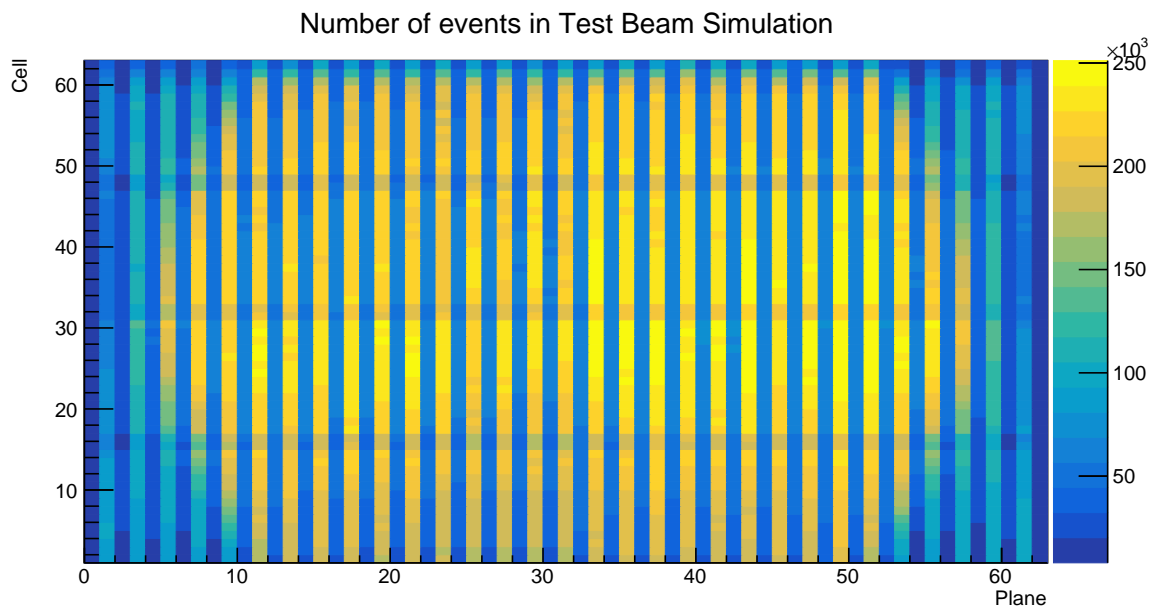


Figure 8: Distribution of events in the Test Beam simulation calibration sample.

pclist samples

Data period 2:

```
prod_pclist_R23-04-05-testbeam-production.a_testbeam_ddactivity1_period2_v1
```

Data period 3:

```
prod_pclist_R23-04-05-testbeam-production.a_testbeam_ddactivity1_epoch3a_v1
```

```
prod_pclist_R23-04-05-testbeam-production.a_testbeam_ddactivity1_epoch3b_v1
```

```
prod_pclist_R23-04-05-testbeam-production.a_testbeam_ddactivity1_epoch3c_v1
```

```
pclist_testbeam_detector_activity_epoch3d_R21-01-28-testbeam-production.a
```

```
pclist_testbeam_detector_activity_epoch3e_R21-01-28-testbeam-production.a
```

Data period 4:

```
prod_pclist_R23-04-05-testbeam-production.a_testbeam_ddactivity1_period4_v1
```

Simulation:

```
rkrilik_pclist_testbeam_databasedsim_R23-04-05-testbeam-production.a
```

pcliststop samples

Data period 2:

```
prod_pcliststop_R23-04-05-testbeam-production.a_testbeam_ddactivity1_period2_v1
```

Data period 3:

```
prod_pcliststop_R23-04-05-testbeam-production.a_testbeam_ddactivity1_epoch3a_v1
```

```
prod_pcliststop_R23-04-05-testbeam-production.a_testbeam_ddactivity1_epoch3b_v1
```

```
prod_pcliststop_R23-04-05-testbeam-production.a_testbeam_ddactivity1_epoch3c_v1
```

```
pcliststop_testbeam_detector_activity_epoch3d_R21-01-28-testbeam-production.a
```

```
pcliststop_testbeam_detector_activity_epoch3e_R21-01-28-testbeam-production.a
```

Data period 4:

```
prod_pcliststop_R23-04-05-testbeam-production.a_testbeam_ddactivity1_period4_v1
```

Simulation:

```
rkrilik_pcliststop_testbeam_databasedsim_R23-04-05-testbeam-production.a
```

Table 2: SAMWEB definitions of the Test Beam calibration samples.

353 **Relative calibration results**

354 **4.4 Threshold and shielding corrections**

355 The threshold and shielding correction for test beam is almost uniform across all cells as can
356 be seen on figure... This is expected as the hight of the Test Beam detector of 2.6m has only a
357 negligible effect on the energy distribution of cosmic muons or on the threshold saturation. The
358 correction is basically just a normalization factor, but since the relative calibration only cares
359 about relative differences across the detector, a normalization factor doesn't change anything.

360 **4.5 Period 1**

361 Only a month of data, only first half of detector filled, primary/secondary beam halo, or over-
362 saturation leading to FEB shutoffs [docdb:38349 and 41331]. Only used for comissioning, not

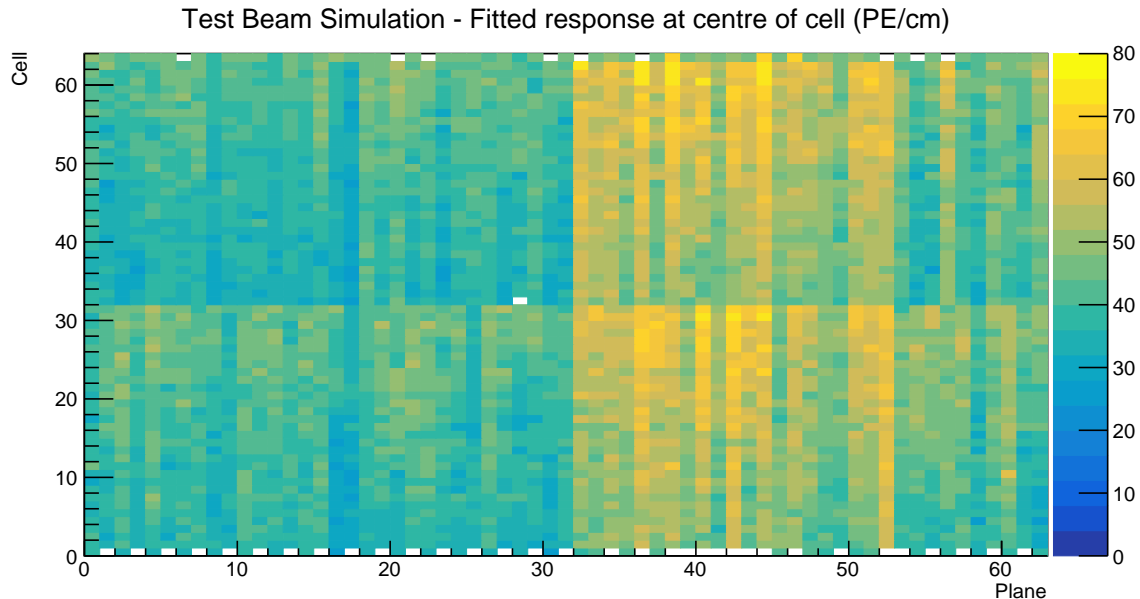


Figure 9: Overview of the relative calibration results for the Teast Beam detector simulation. Each cell represents the result fo the attenuation fit to the energy response in the centre of that cell. The blank cells are uncalibrated.

³⁶³ used for any data analysis or calibration.

³⁶⁴ 4.6 Period 2

³⁶⁵ What was done for the period 2 tb calibration, short overview of what has been done: test beam
³⁶⁶ data were calibrated all at the same time without splitting them to separate epochs. See figures
³⁶⁷ [12](#), [13](#) and [14](#).

³⁶⁸ 4.6.1 Relative calibration results

³⁶⁹ 4.7 Period 3

³⁷⁰ Separation of Period 3 data into different epochs based on the running conditions (include plot
³⁷¹ of the running conditions). We are separating data into pre- and post- filling states. We're using
³⁷² only the fully-refilled post-FEB swap data from period 3 as a basis for the simulation creation.

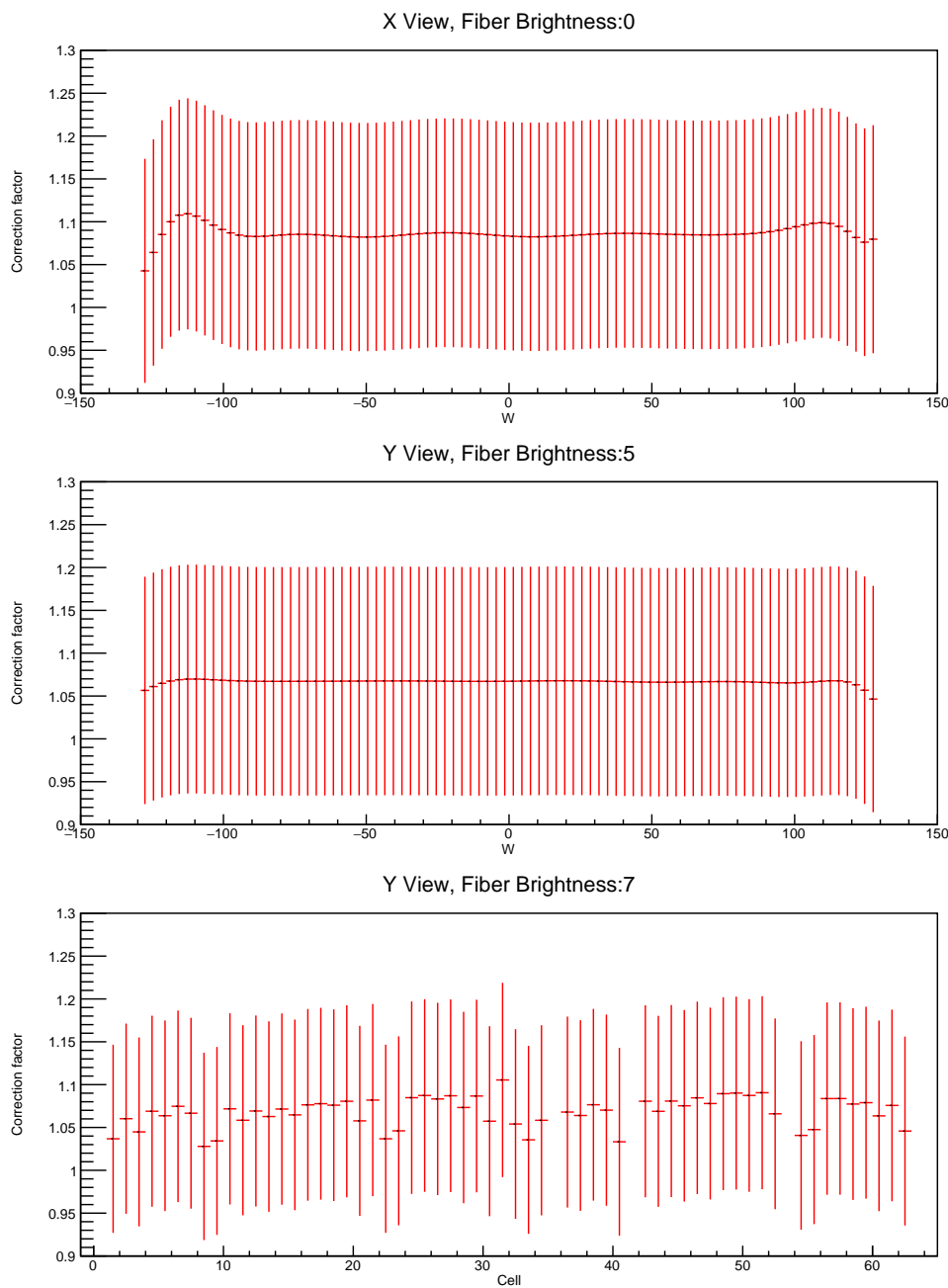


Figure 10: Examples of threshold and shielding corrections for the Test Beam detector

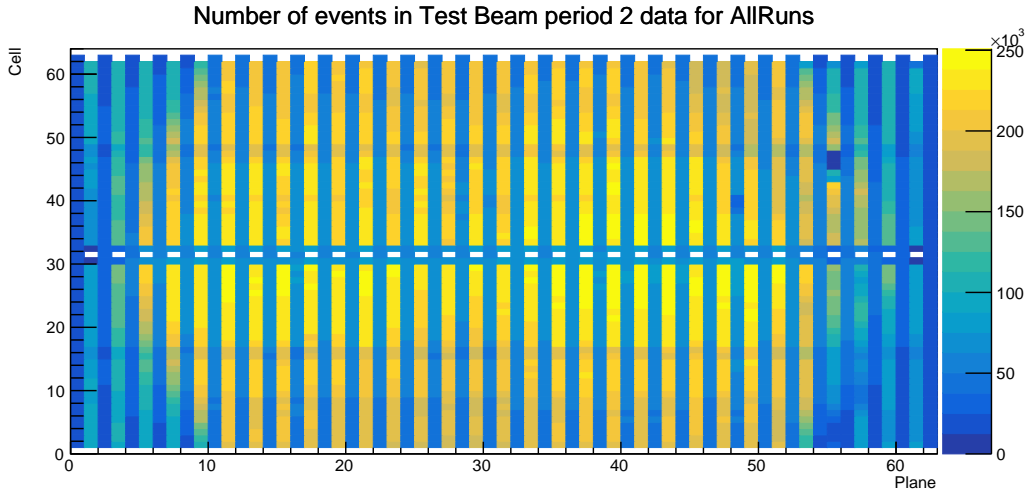


Figure 11: Distribution of events in the period 2 Test Beam data calibration sample.

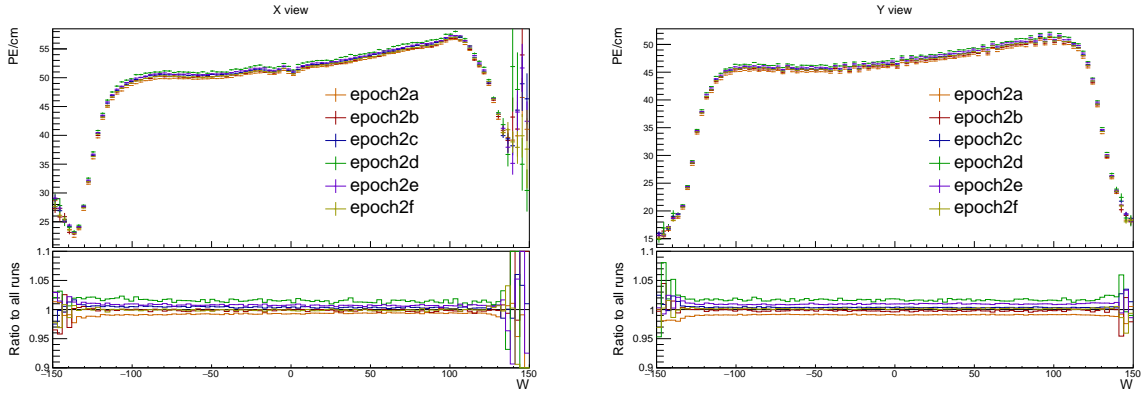


Figure 12: Uncorrected average energy response as a function of the position within a cell (w) for epochs in period 2. It is clear that there is no significant difference between the various epochs.

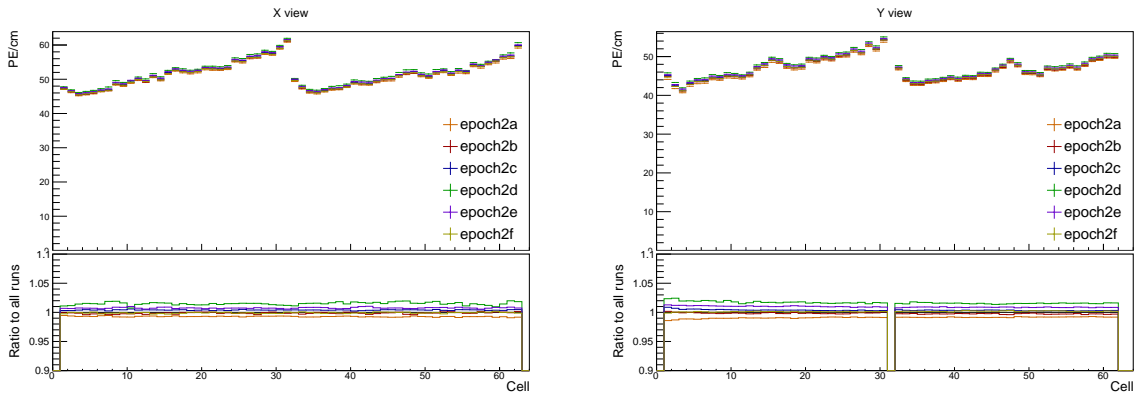


Figure 13: Uncorrected average energy response as a function of cells for epochs in period 2.

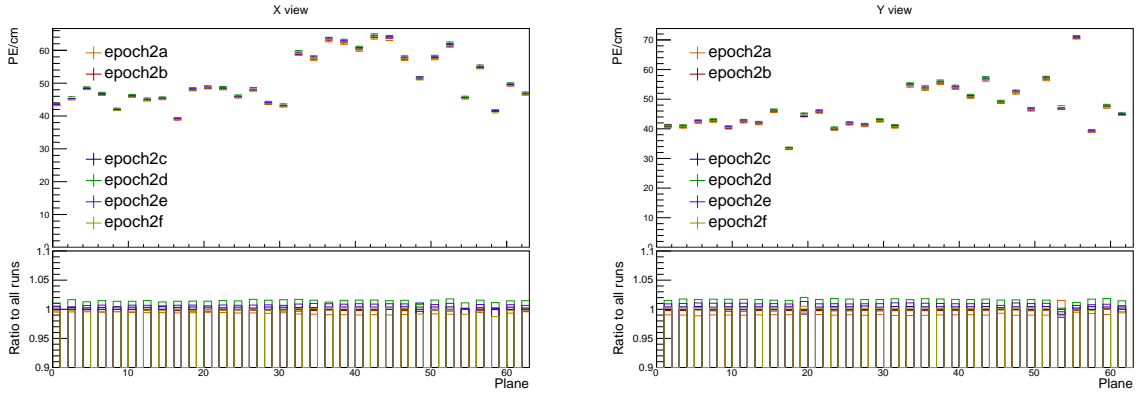


Figure 14: Uncorrected average energy response as a function of planes for epochs in period 2.

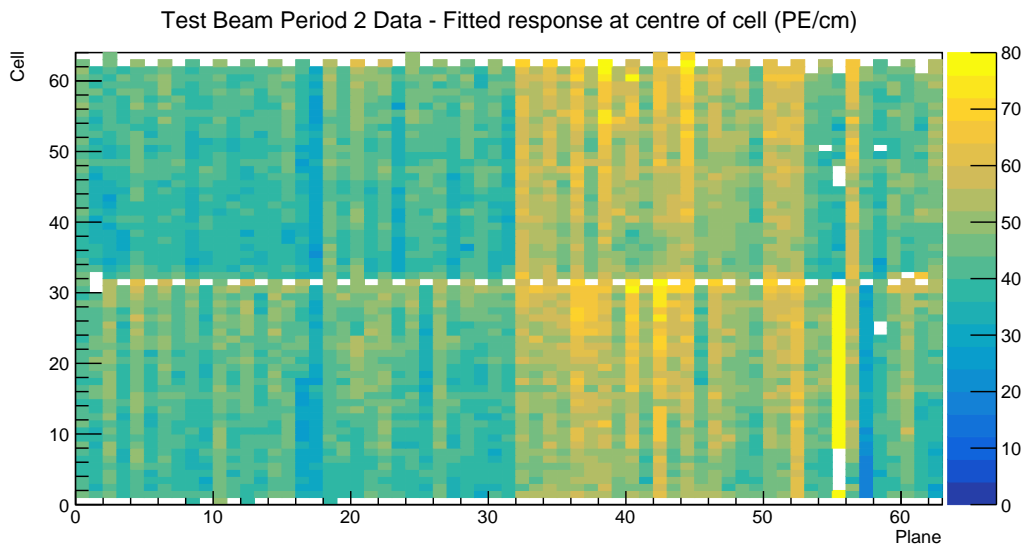


Figure 15: Overview of the relative calibration results for the Teast Beam detector period 2 data. Each cell represents the result fo the attenuation fit to the energy response in the centre of that cell. The blank cells are uncalibrated.

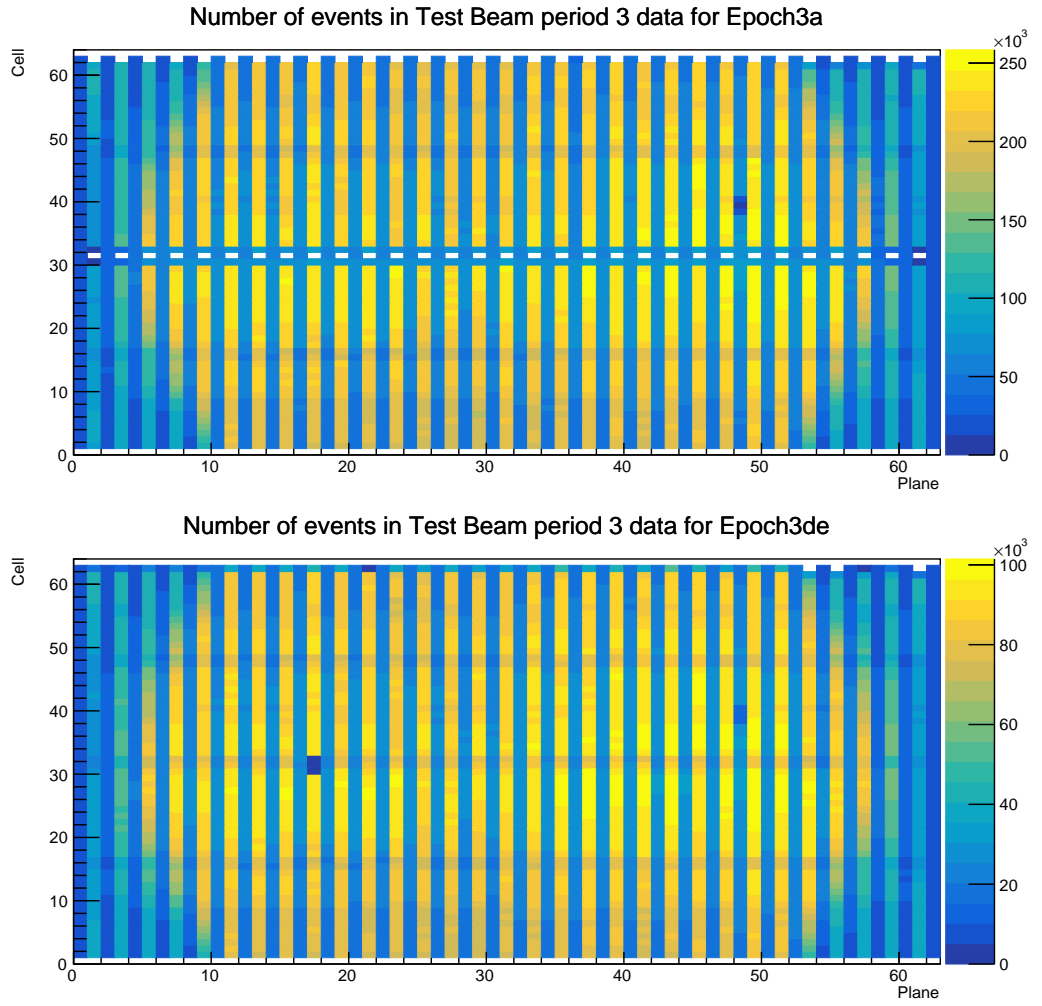


Figure 16: Distribution of events in the period 3, epoch 3a Test Beam data calibration sample.

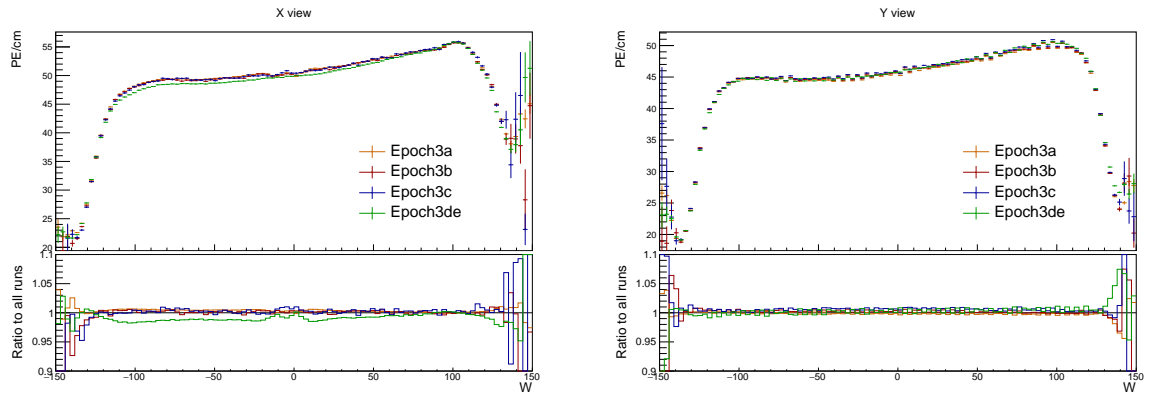


Figure 17: Uncorrected average energy response as a function of the position within a cell (w) for epochs in period 3.

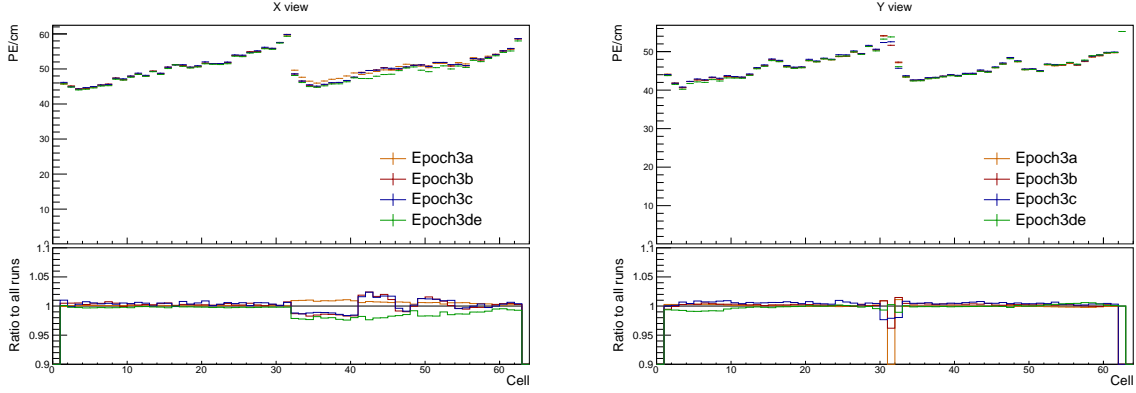


Figure 18: Uncorrected average energy response as a function of cells for epochs in period 3.

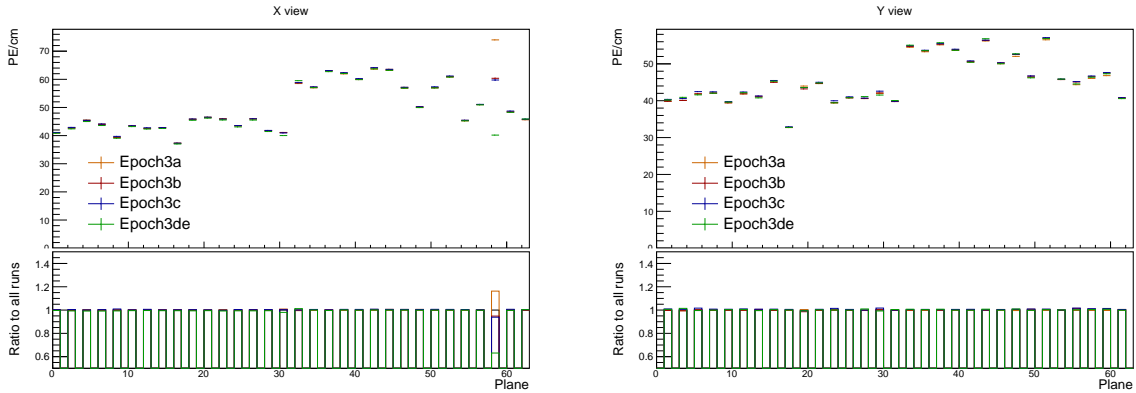


Figure 19: Uncorrected average energy response as a function of planes for epochs in period 3.

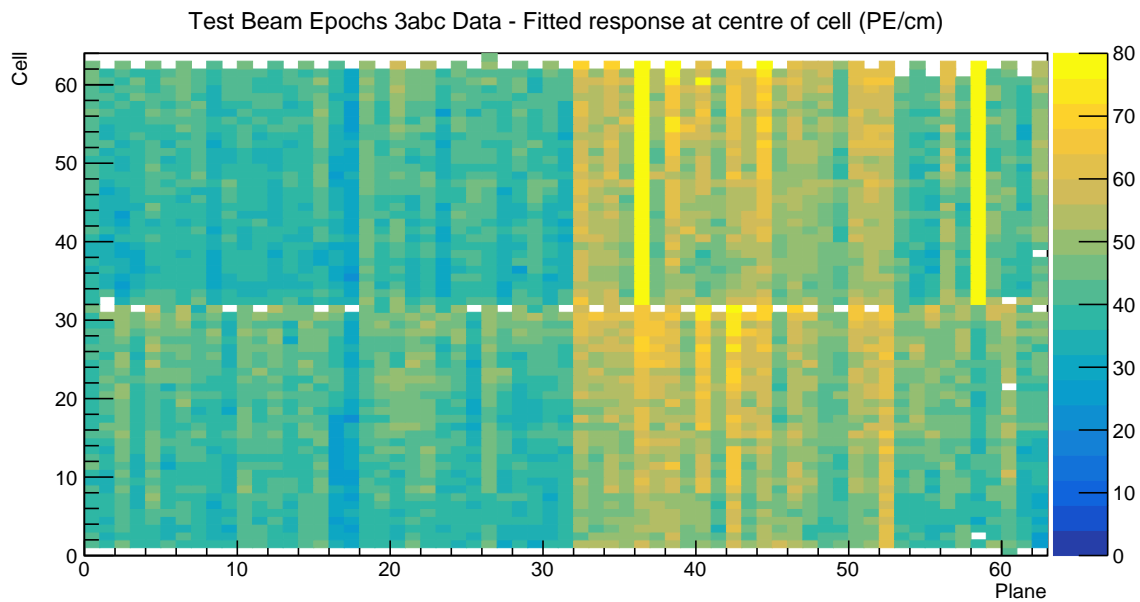


Figure 20: Overview of the relative calibration results for the Teast Beam detector period 3, combined epochs 3a, 3b and 3c data. Each cell represents the result fo the attenuation fit to the energy response in the centre of that cell. The blank cells are uncalibrated.

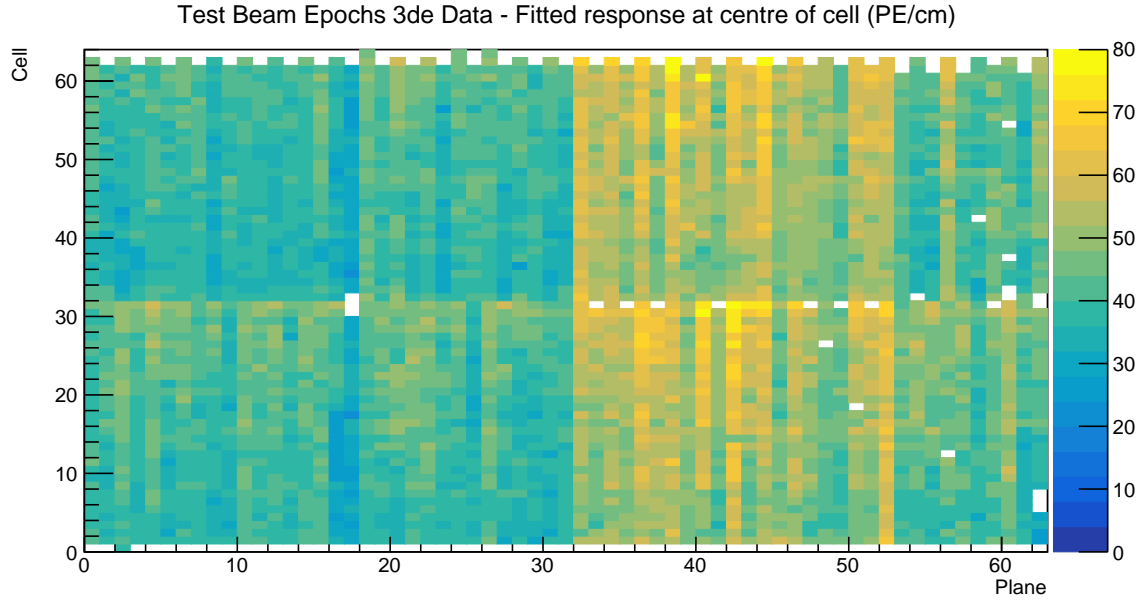


Figure 21: Overview of the relative calibration results for the Teast Beam detector period 3, combined epochs 3d and 3e data. Each cell represents the result fo the attenuation fit to the energy response in the centre of that cell. The blank cells are uncalibrated.

³⁷³ **4.7.1 Relative calibration results**

³⁷⁴ **Combined epochs 3a, 3b and 3c**

³⁷⁵ **Combined epochs 3d and 3e**

³⁷⁶ **4.8 Period 4**

³⁷⁷ **4.8.1 Relative calibration results**

³⁷⁸ **4.9 Absolute calibration results**

³⁷⁹ Standard absolute calibration cuts: track window, flat-response W, positive pe, pecorr, and
³⁸⁰ pathlenght reco

Sample	NHitsx	MEUx	NHitsy	MEUy	MEU	MEU Err	TrueE/dx	tE/dx Err
epoch 3abc data	2.638e+05	38.49	1.621e+06	39.4	38.94	0.006758	1.772	0.000238
epoch 3de data	1.049e+05	38.63	6.725e+05	39.42	39.02	0.01048	1.772	0.000238
period 2 data	2.322e+05	38.7	1.413e+06	39.4	39.05	0.007252	1.772	0.000238
period 4 data	5.268e+05	38.63	3.316e+06	39.4	39.01	0.004703	1.772	0.000238
simulation	2.829e+05	40.17	1.842e+06	39.93	40.05	0.006418	1.772	0.000238

³⁸¹

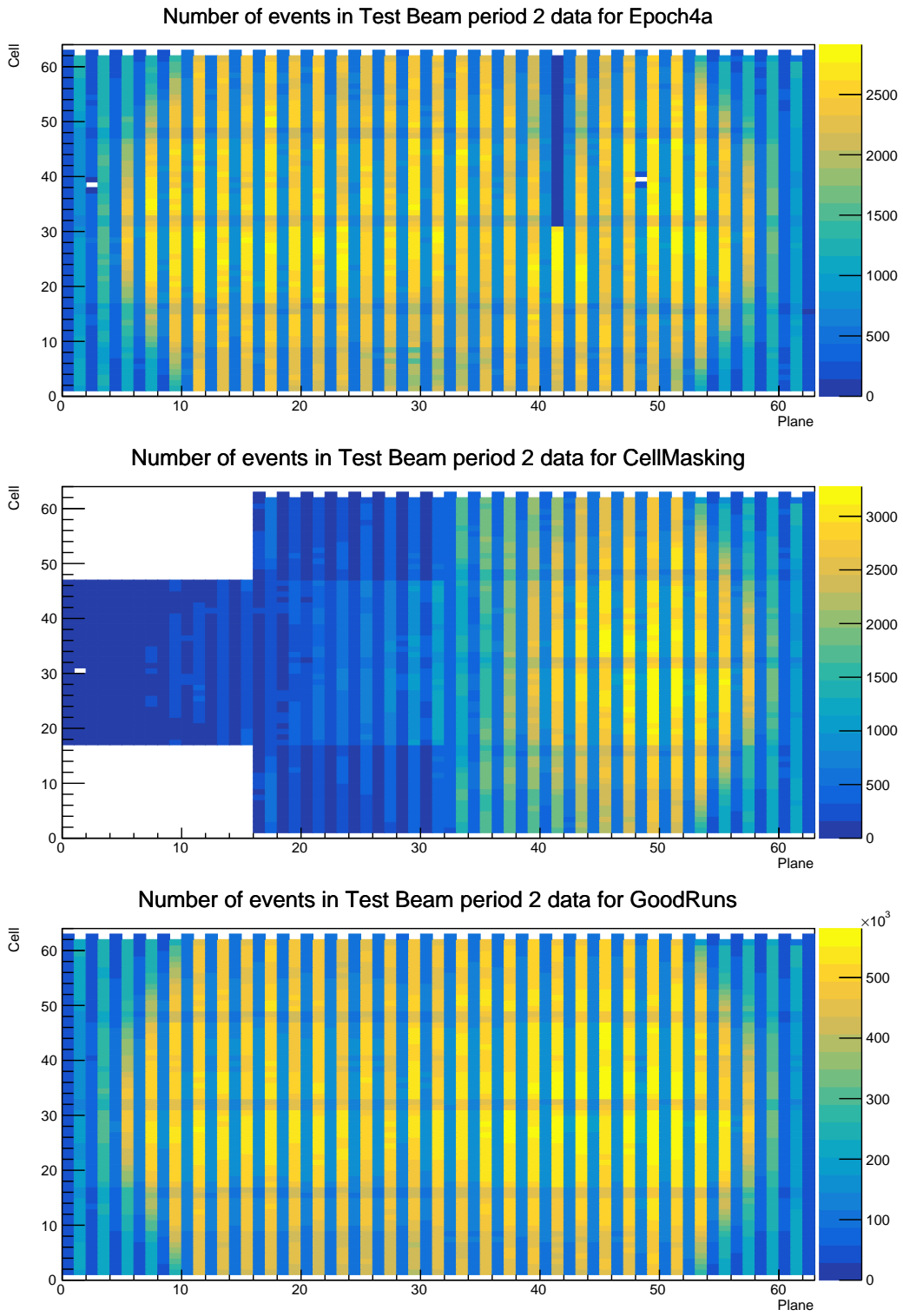


Figure 22: Distribution of events in the Test Beam period 4 data calibration sample. The top plot shows the first three commissioning runs, the middle plot the status of the detector during the Cell Masking studies and the bottom plot shows the rest.

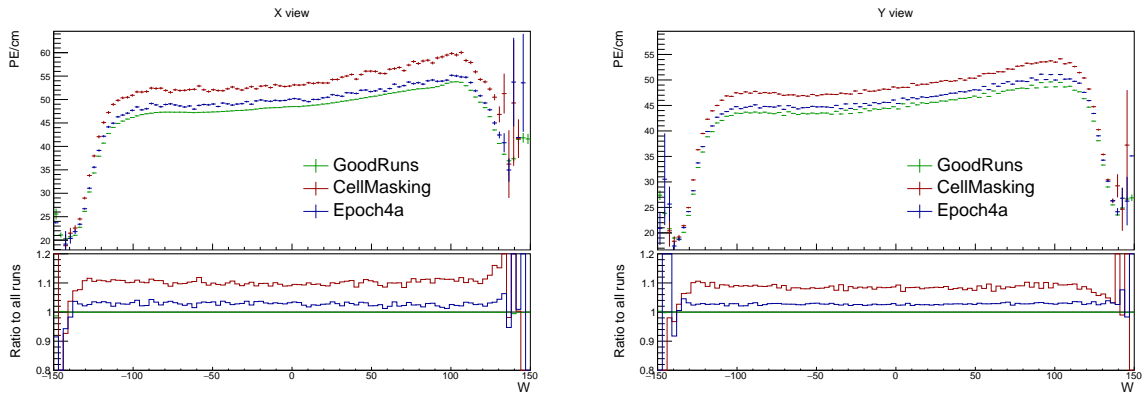


Figure 23: Uncorrected average energy response as a function of the position within a cell (w) for epochs in period 4.

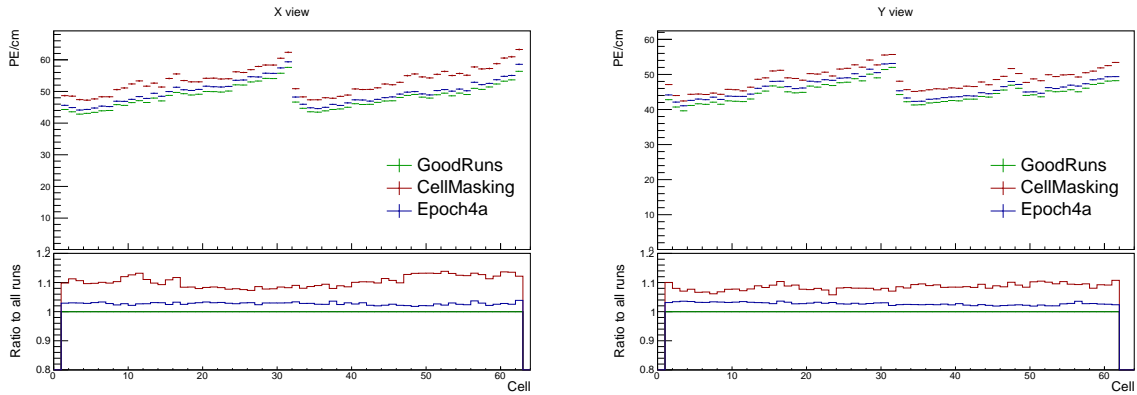


Figure 24: Uncorrected average energy response as a function of cells for epochs in period 4.

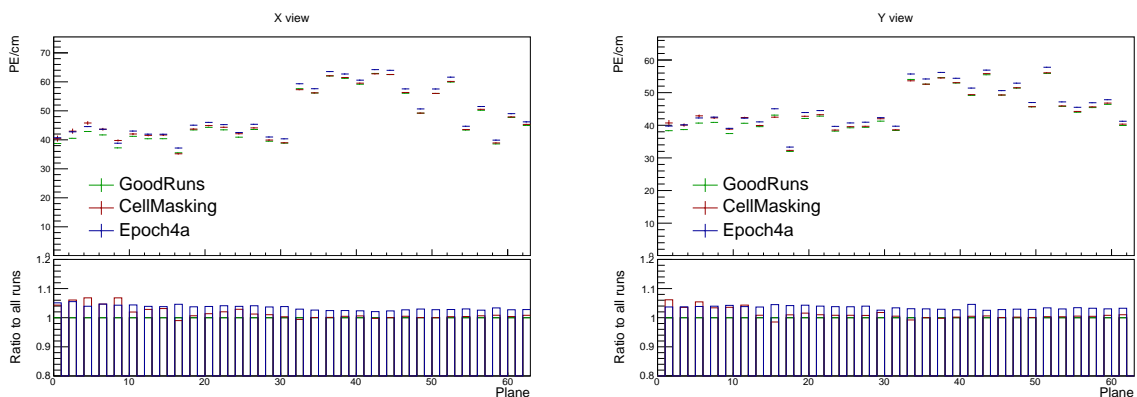


Figure 25: Uncorrected average energy response as a function of planes for epochs in period 4.

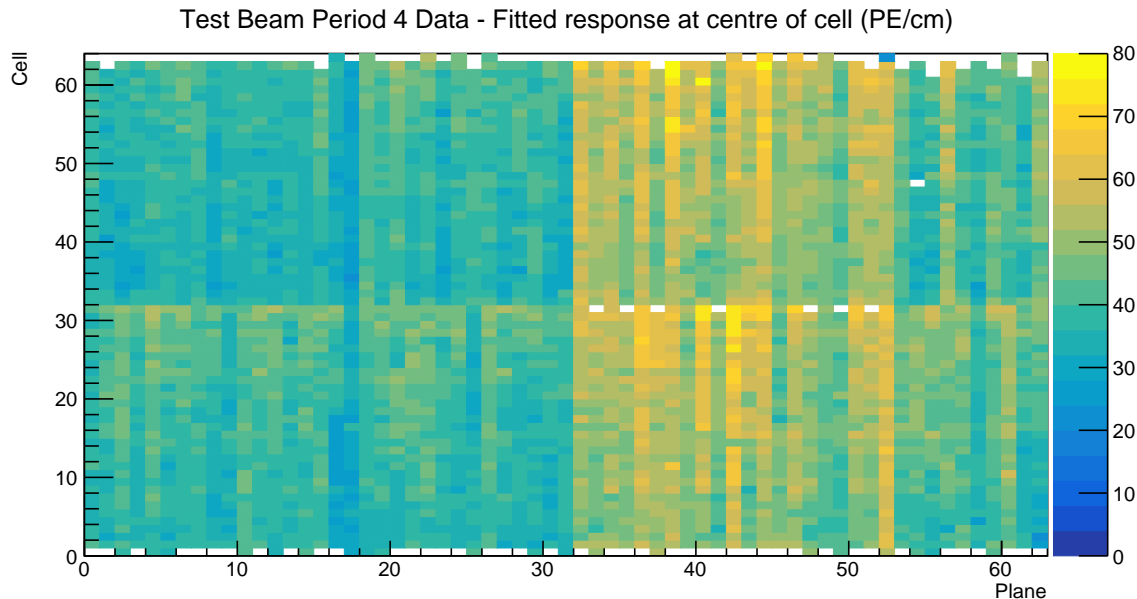


Figure 26: Overview of the relative calibration results for the Teast Beam detector period 4 data. Each cell represents the result fo the attenuation fit to the energy response in the centre of that cell. The blank cells are uncalibrated.

382 4.10 Drift in TB data

383 4.11 Results

384 Table of final results. Final CSVs are locate in the /nova/ana/testbeam/calibration and
385 they have been included in the vXX.XX calibration tag.
386 Plots of absolute calibration results

387 4.12 Validation

388 Comparisons with older version of calibration and maybe with the FD and ND

389 References

- 390** [1] Michael Wallbank. The NOvA Test Beam Program. *PoS*, ICHEP2020:188, 2021. [doi: 10.22323/1.390.0188](https://doi.org/10.22323/1.390.0188).
- 392** [2] Alex Sousa. NOvA Test Beam Status and Plans - Support Documentation. NOVA Document 22172-v2, October 2017. NOvA technical note. URL: <https://nova-docdb.fnal.gov/cgi-bin/sso>ShowDocument?docid=22172>.
- 395** [3] Alex Sousa. NOvA Test Beam Plenary @ IU Collaboration Meeting. NOVA Document 29543, May 2018. NOvA internal document. URL: <https://nova-docdb.fnal.gov/cgi-bin/sso>ShowDocument?docid=29543>.

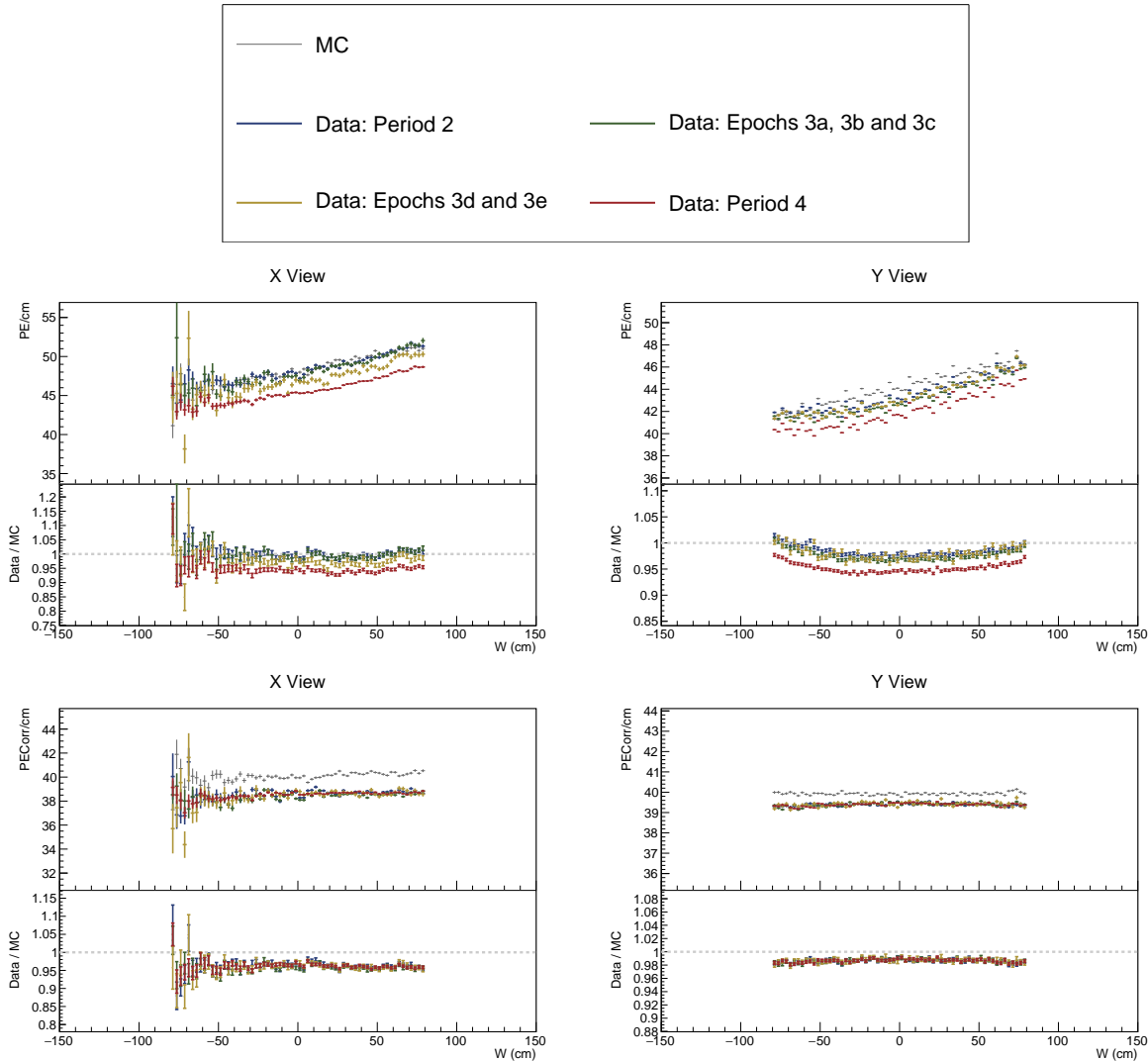


Figure 27: ...

- 398 [4] Michael Wallbank. Final Test Beam Updates (Geometry and Other!). NOVA Document
 399 58388, April 2023. NOvA internal document. URL: <https://nova-docdb.fnal.gov/cgi-bin/sso>ShowDocument?docid=58388>.
- 400
- 401 [5] Michael Wallbank. Understanding, Improving, Validating the Test Beam Geometry.
 402 NOVA Document 57955, February 2023. NOvA internal document. URL: <https://nova-docdb.fnal.gov/cgi-bin/sso>ShowDocument?docid=57955>.
- 403
- 404 [6] Robert Kralik. Test beam calibration update. NOVA Document 57516-v2, January
 405 2023. NOvA internal document. URL: <https://nova-docdb.fnal.gov/cgi-bin/sso>ShowDocument?docid=57516>.
- 406
- 407 [7] Alex Sousa. Test Beam Scintillator Fill Plan. NOVA Document 34196, November
 408 2018. NOvA internal document. URL: <https://nova-docdb.fnal.gov/cgi-bin/sso>ShowDocument?docid=34196>.
- 409

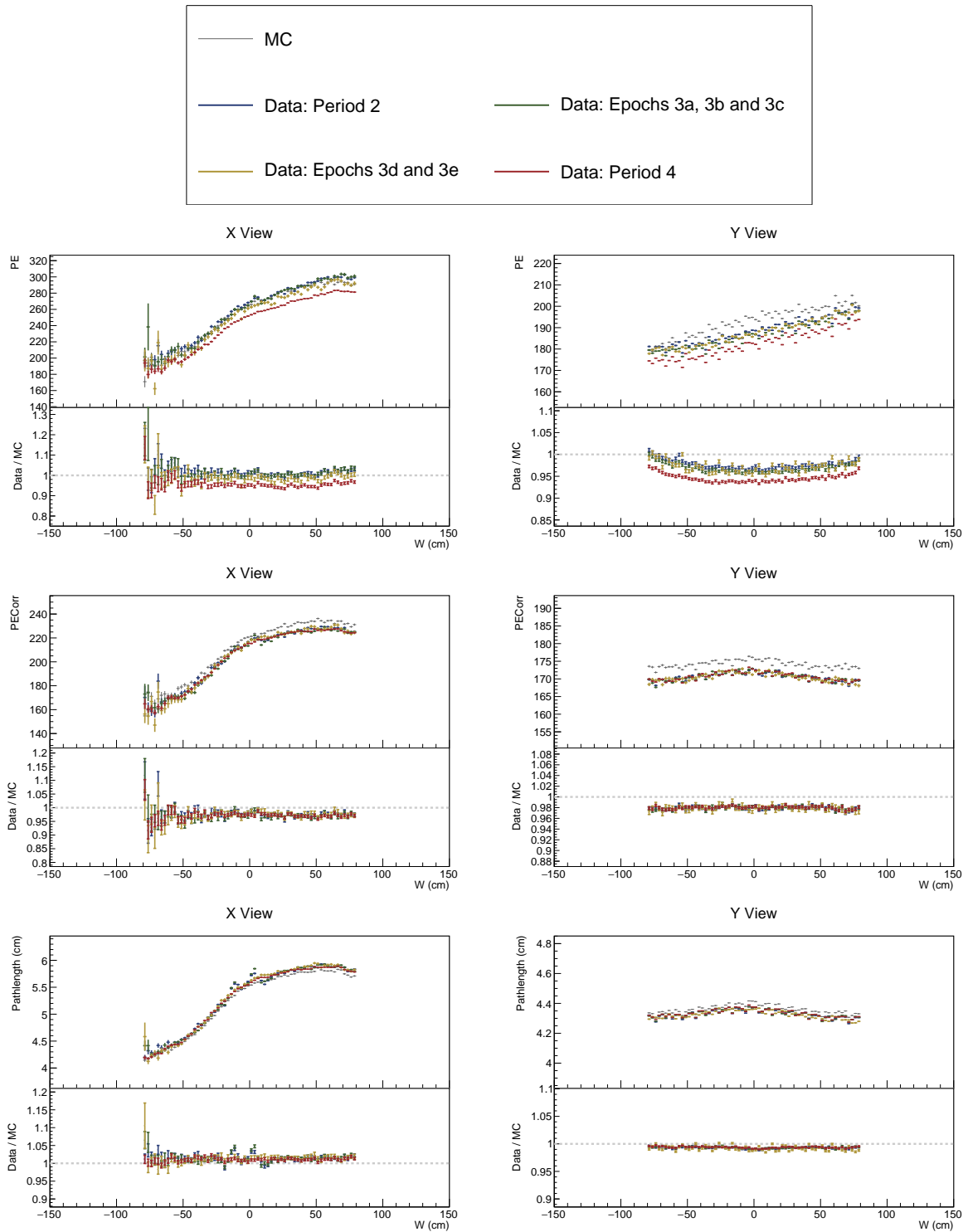


Figure 28: ...

- 410 [8] Alex Sousa. Test Beam Plenary Update - Jun. 6, 2019. NOVA Document 38349, June
 411 2019. NOvA internal document. URL: <https://nova-docdb.fnal.gov/cgi-bin/sso>ShowDocument?docid=38349>.
- 412
- 413 [9] Alex Sousa. Test Beam Plenary Update - FNAL September 2018. NOVA Document

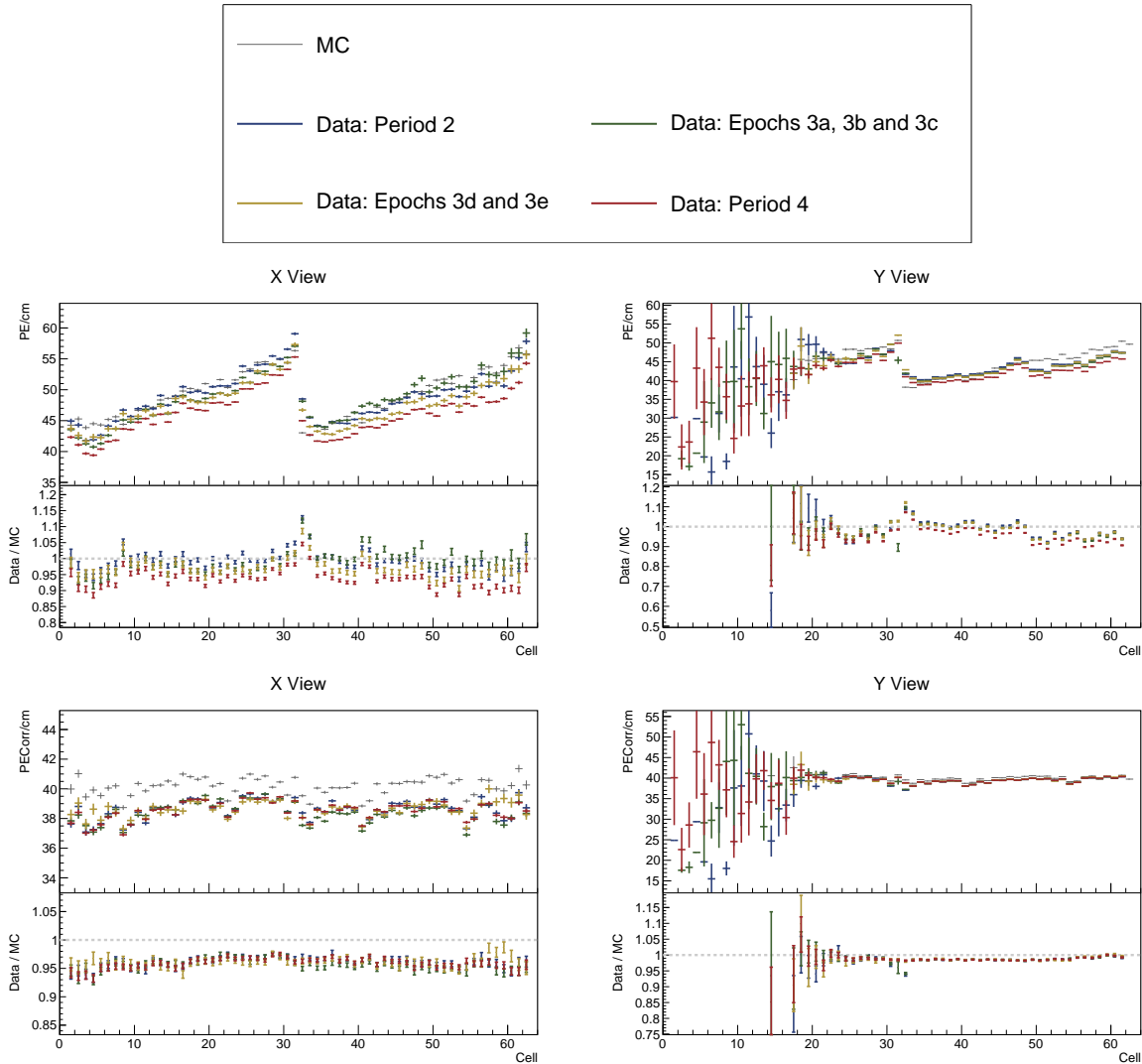


Figure 29: ...

33012, September 2018. NOvA internal document. URL: <https://nova-docdb.fnal.gov/cgi-bin/sso>ShowDocument?docid=33012>.

- 414 [10] Karol Lang. NOvA Test Beam: To mix, or not to mix, that is the question. NOVA Document
415 34046-v2, November 2018. NOvA technical note. URL: <https://nova-docdb.fnal.gov/cgi-bin/sso>ShowDocument?docid=34046>.
- 419 [11] Alex Sousa. 2nd Block Filling Status - Nov. 18, 2019. NOVA Document 41961, November
420 2019. NOvA internal document. URL: <https://nova-docdb.fnal.gov/cgi-bin/sso>ShowDocument?docid=41961>.
- 422 [12] Alex Sousa. Filling System and Scintillator Status. NOVA Document 34067, November
423 2018. NOvA internal document. URL: <https://nova-docdb.fnal.gov/cgi-bin/sso>ShowDocument?docid=34067>.
- 425 [13] Junting Huang, Will Flanagan, and Beatriz Tapia Oregui. Test Beam: Light Yield of
426 the Liquid Scintillator Drained from the NDOS Detector. NOVA Document 38740, July

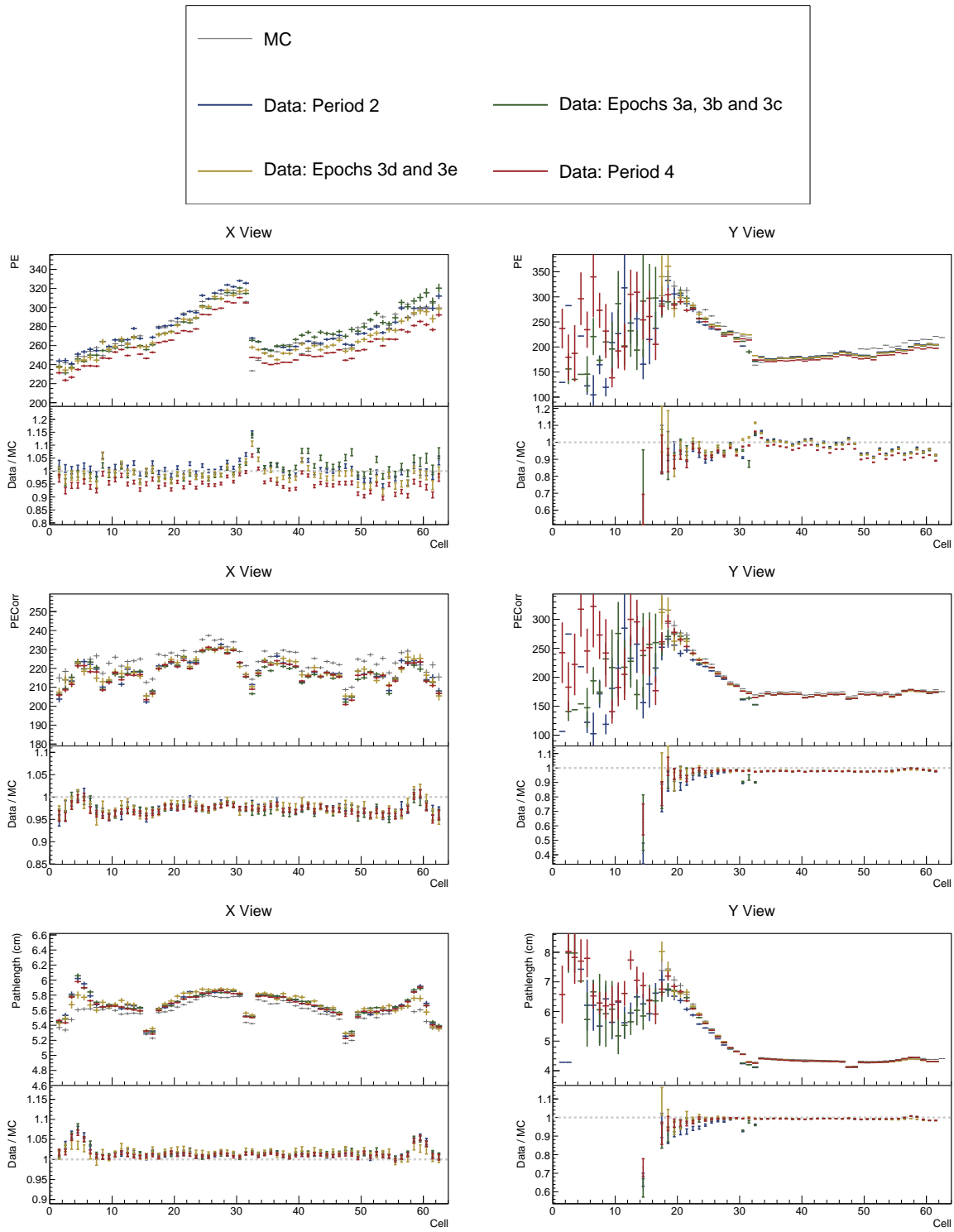


Figure 30: ...

427 2019. NOvA internal document. URL: <https://nova-docdb.fnal.gov/cgi-bin/sso>ShowDocument?docid=38740>.

429 [14] Dung Phan. Test Beam: Tintometer Measurement of Texas A&M oil. NOVA Document
430 39088, July 2019. NOvA internal document. URL: <https://nova-docdb.fnal.gov/>

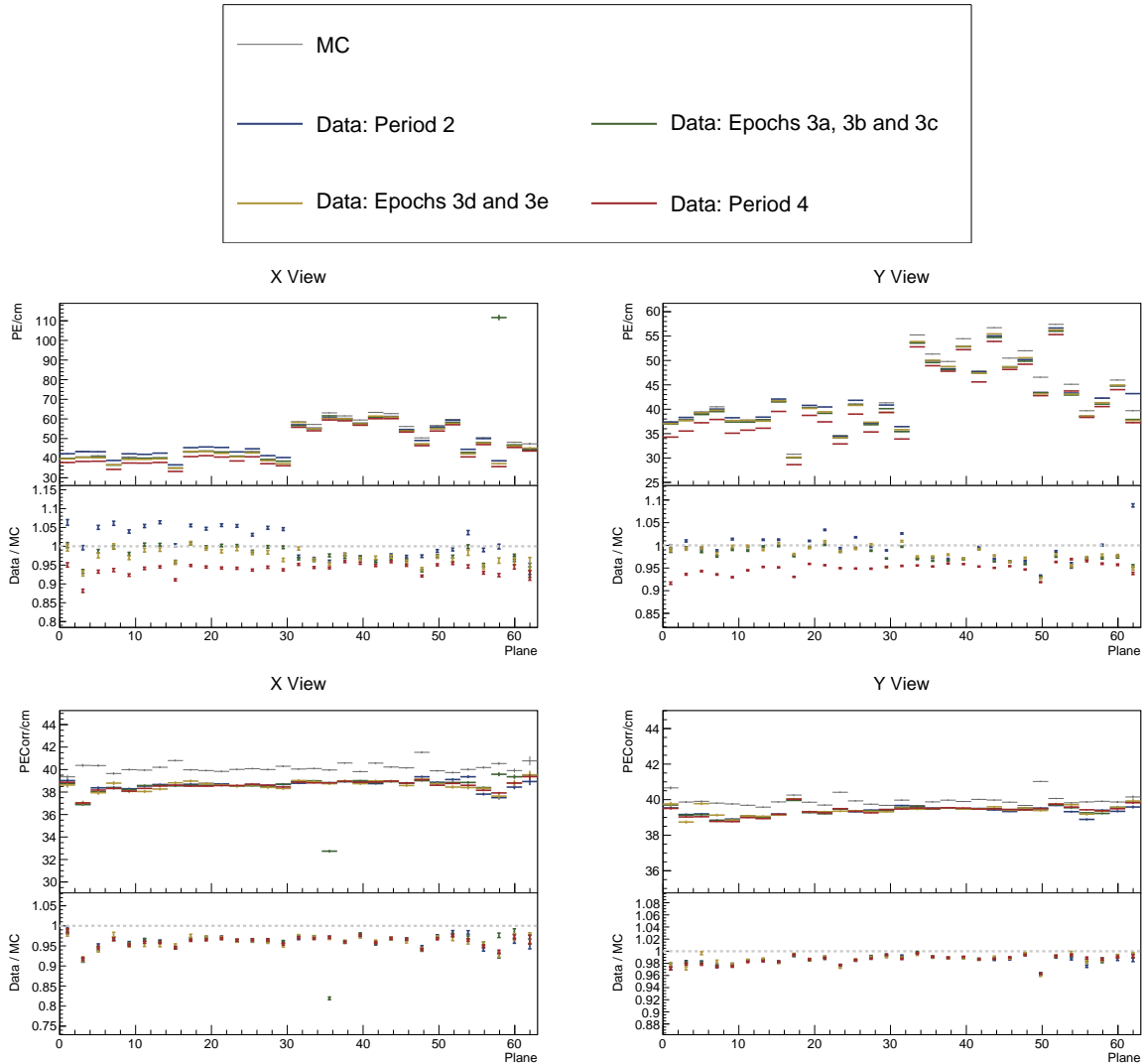


Figure 31: ...

431 [cgi-bin/sso>ShowDocument?docid=39088](https://nova-docdb.fnal.gov/cgi-bin/sso>ShowDocument?docid=39088).

- 432 [15] Teresa Megan Lackey. *Proton Scattering in NOvA Test Beam*. PhD thesis, Indiana U.,
433 July 2022.
- 434 [16] David Northacker, Alex Sousa, and Yagmur Torun. Test Beam - Overfilling Horizontal
435 Planes. NOVA Document 49439, March 2021. NOvA internal document. URL: <https://nova-docdb.fnal.gov/cgi-bin/sso>ShowDocument?docid=49439>.
- 436
- 437 [17] Keith Matera et al. Calibration Technotes. NOVA Document 13579, January
438 2017. NOvA technical note. URL: <https://nova-docdb.fnal.gov/cgi-bin/sso>ShowDocument?docid=13579>.
- 439
- 440 [18] Christopher J. Backhouse. Cell-by-cell attenuation calibration of the NOvA detectors.
441 NOVA Document 7410, December 2014. NOvA technical note. URL: <https://nova-docdb.fnal.gov/cgi-bin/sso>ShowDocument?docid=7410>.
- 442

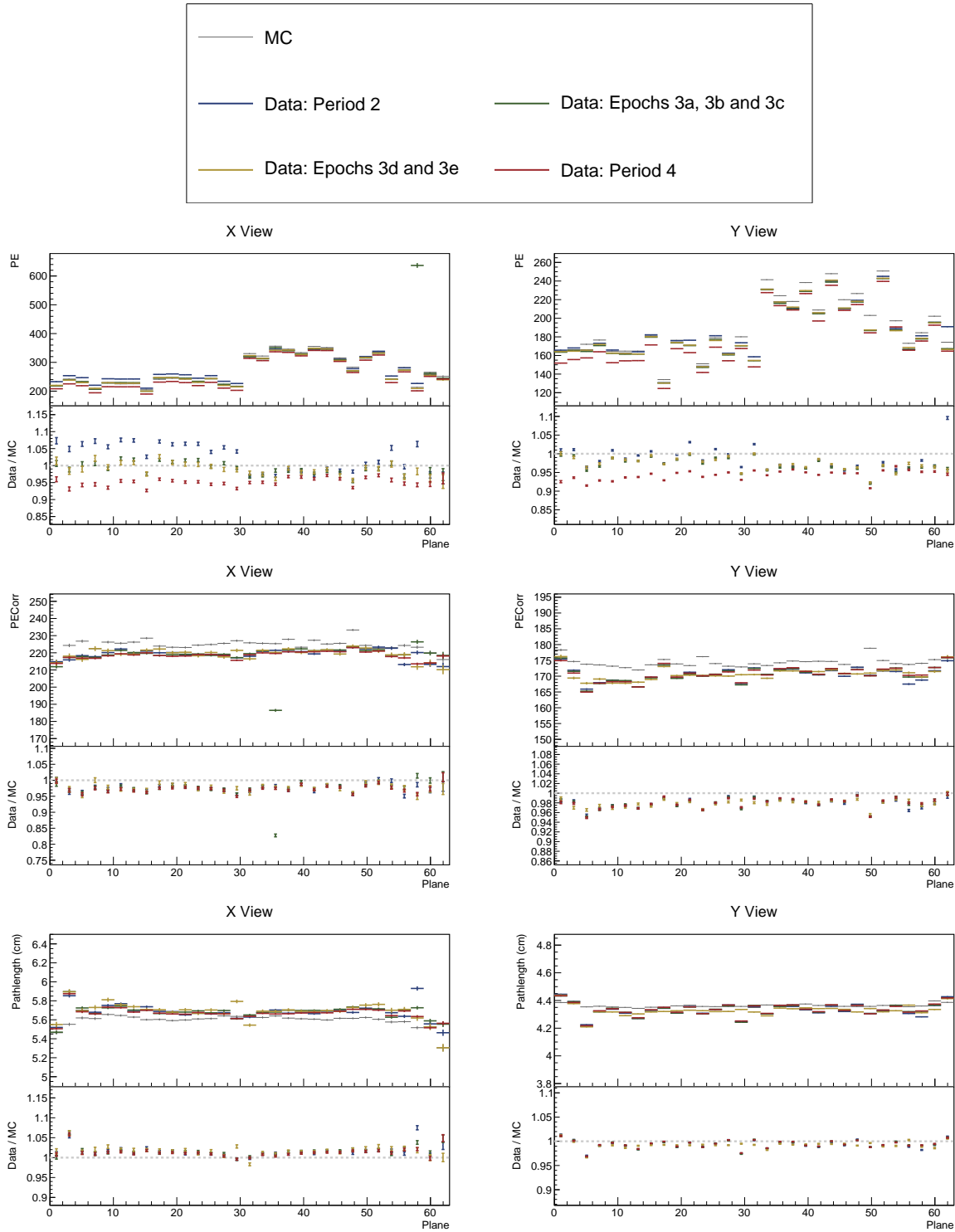


Figure 32: ...

- 443 [19] Evan David Niner. *Observation of Electron Neutrino Appearance in the NuMI Beam with*
 444 *the NOvA Experiment*. PhD thesis, Indiana U., 2015. doi:10.2172/1221353.
- 445 [20] Christopher J. Backhouse. Timing bias introduced by incorrect interpretation of the
 446 nanoslice. NOVA Document 13518, June 2015. NOvA technical note. URL: [https:](https://)

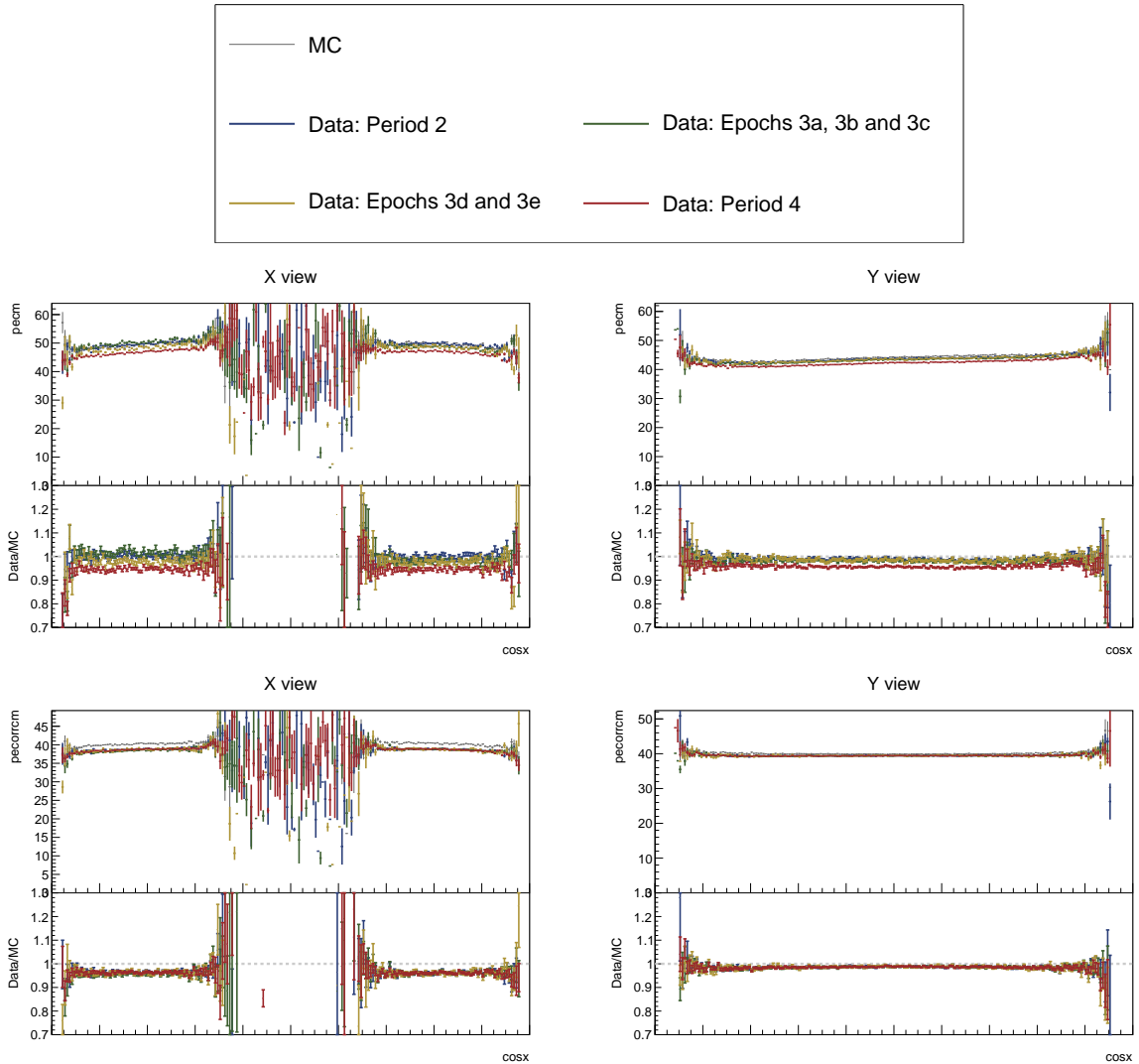


Figure 33: ...

447 [//nova-docdb.fnal.gov/cgi-bin/sso>ShowDocument?docid=13518](https://nova-docdb.fnal.gov/cgi-bin/sso>ShowDocument?docid=13518).

- 448 [21] Luke Vinton. Calorimetric Energy Scale Calibration of the NOvA Detectors. NOVA Document 13579, document FA_Calorimetric_energy_scale.pdf, July 2015. NOvA technical note. URL: <https://nova-docdb.fnal.gov/cgi-bin/sso>ShowDocument?docid=13579>.
- 449
450
451
- 452 [22] Keith Matera. Keith's Swell Guide: The Calibration Meta. NOVA Document 13579, document Calibration_Meta_READFIRST.pdf, January 2017. NOvA technical note. URL: <https://nova-docdb.fnal.gov/cgi-bin/sso>ShowDocument?docid=13579>.
- 453
454
- 455 [23] Christopher Backhouse, Alexender Radovic, and Prabhjot Singh. The Attenuation and Threshold Calibration of the NOvA detectors. NOVA Document 13579, document SA_Attenuation_and_Threshold.pdf, May 2016. NOvA technical note. URL: <https://nova-docdb.fnal.gov/cgi-bin/sso>ShowDocument?docid=13579>.
- 456
457
458

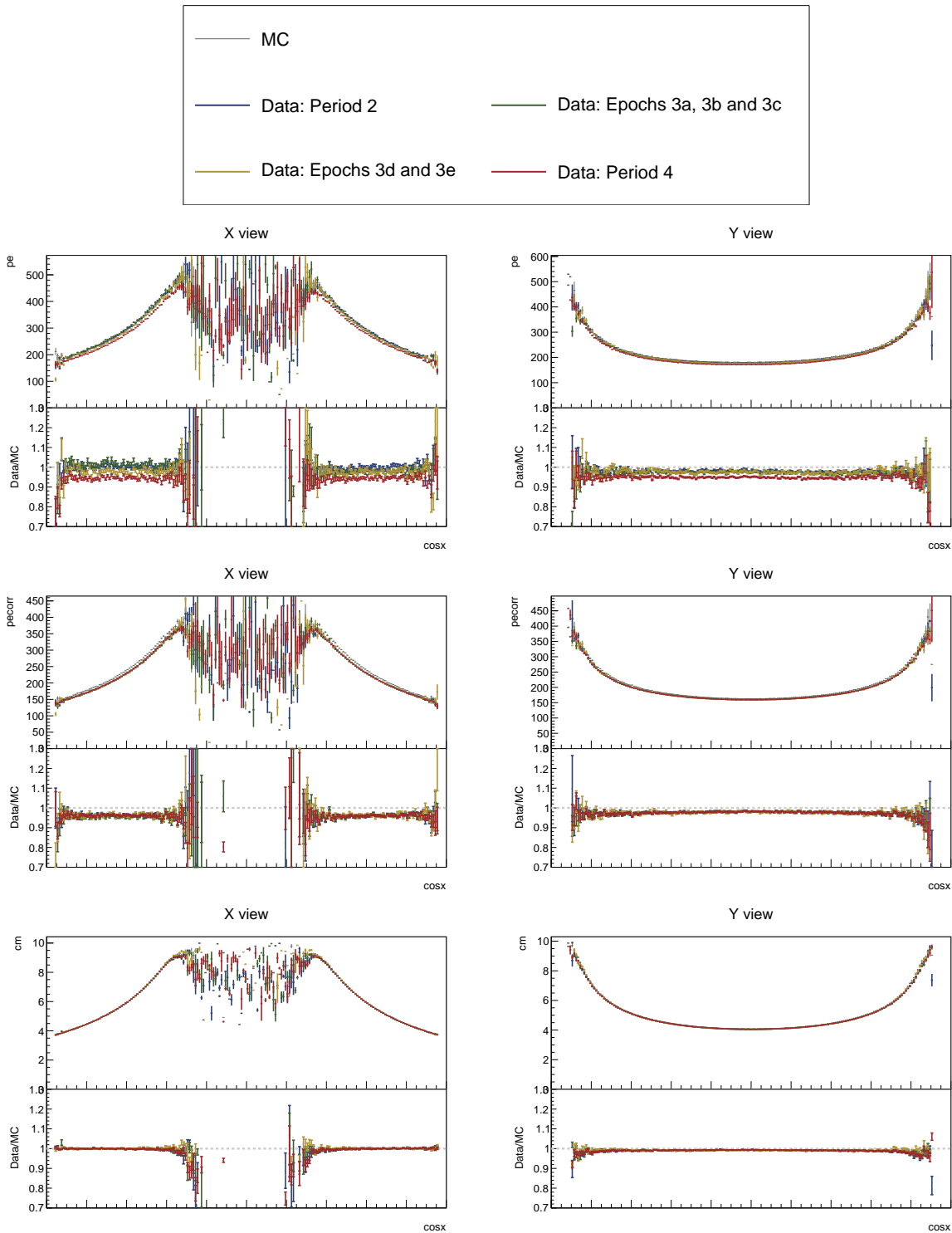


Figure 34: ...

- 459 [24] Ryan J. Nichol. Fibre brightness from cosmic muon data. NOVA Document 34909, De-
 460 cember 2018. NOvA technical note. URL: <https://nova-docdb.fnal.gov/cgi-bin/sso>ShowDocument?docid=34909>.

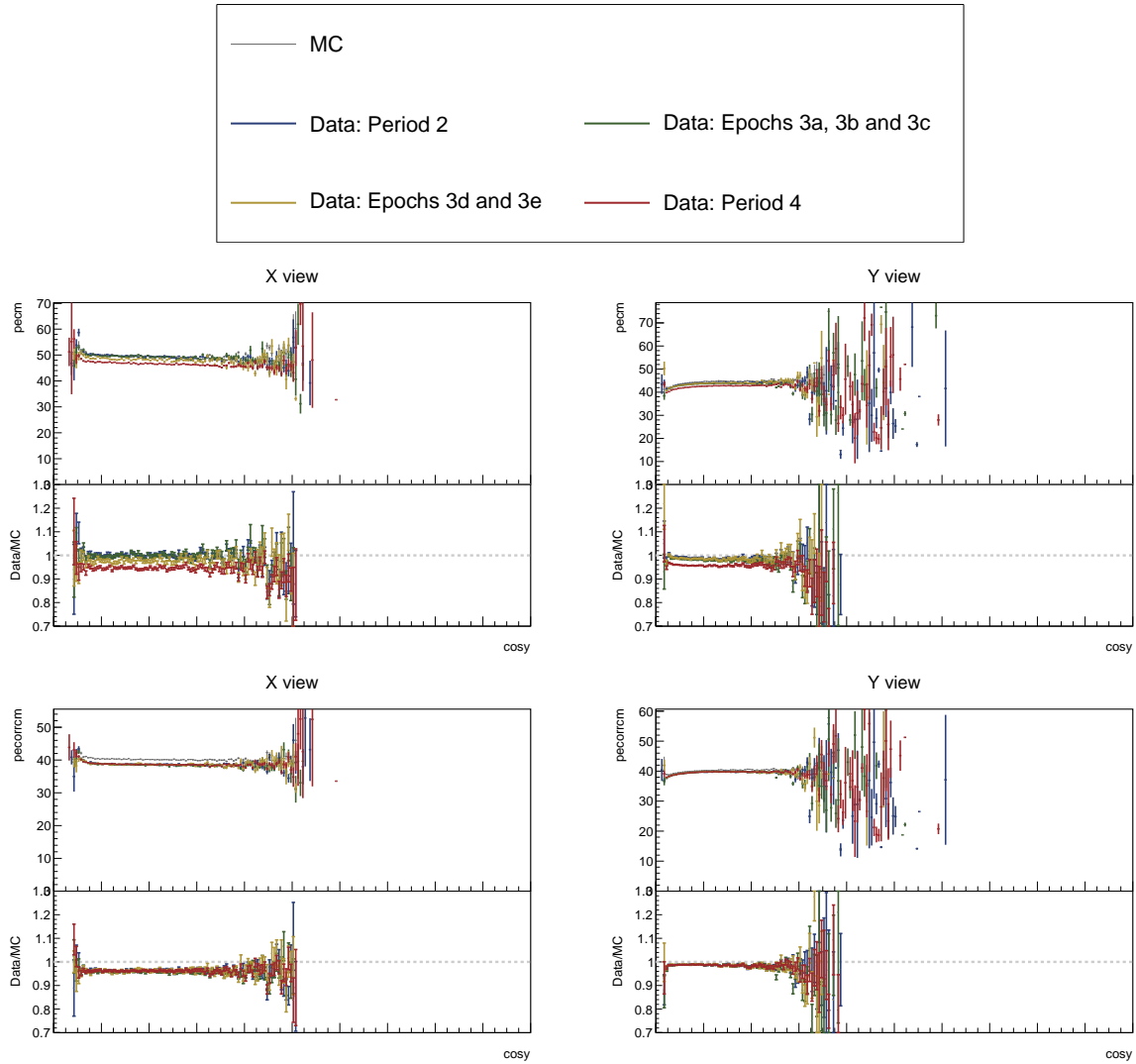


Figure 35: ...

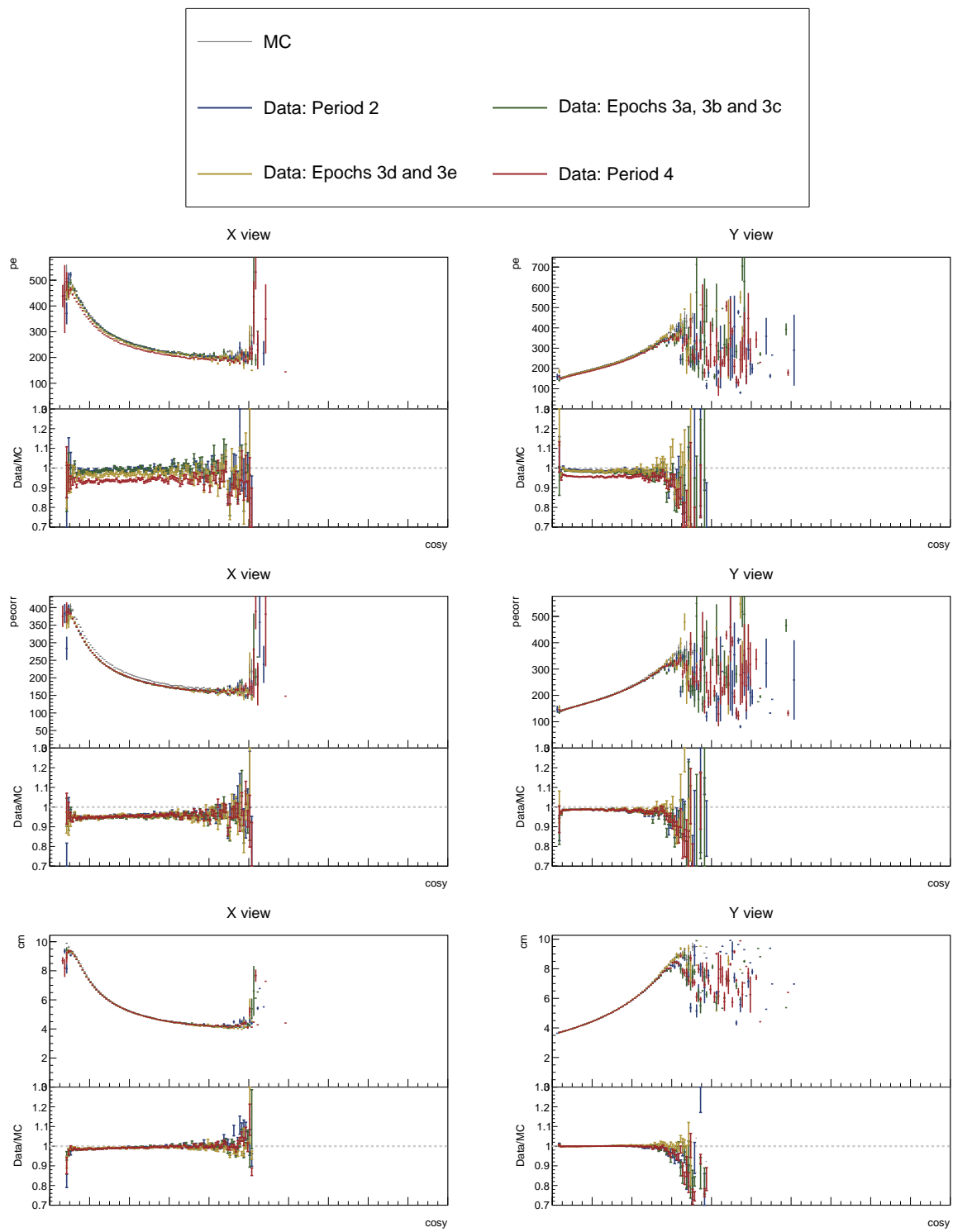


Figure 36: ...

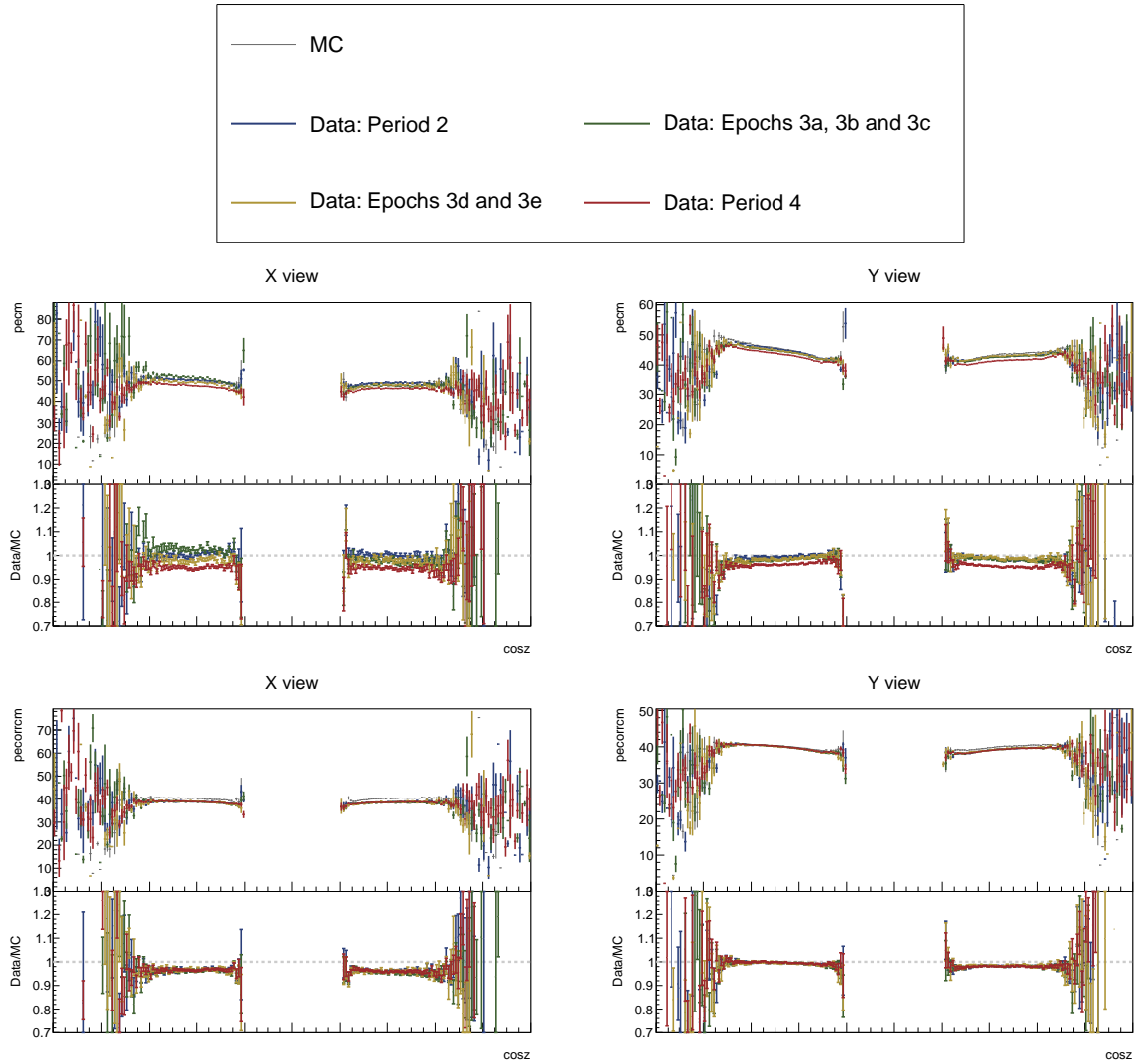


Figure 37: ...

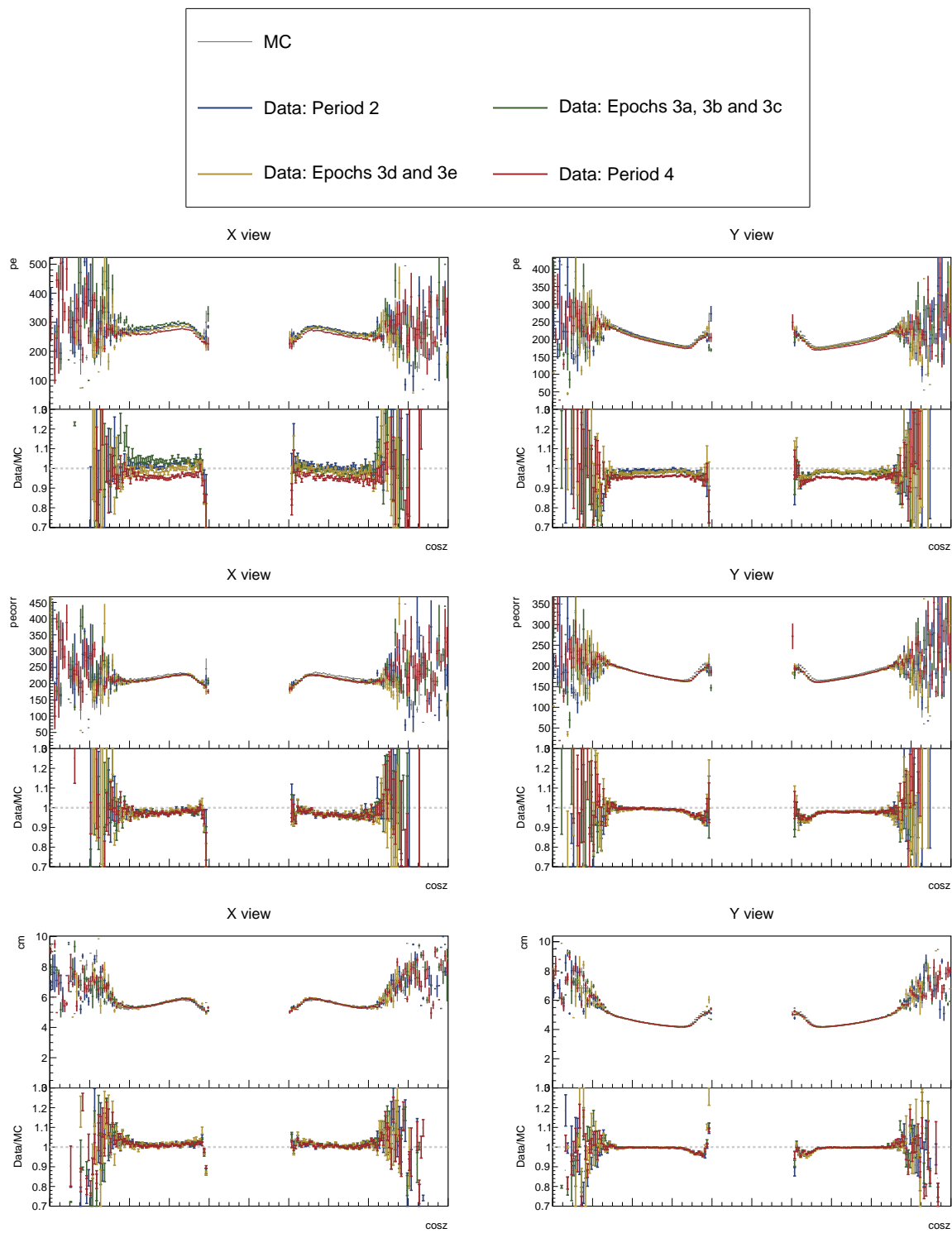


Figure 38: ...

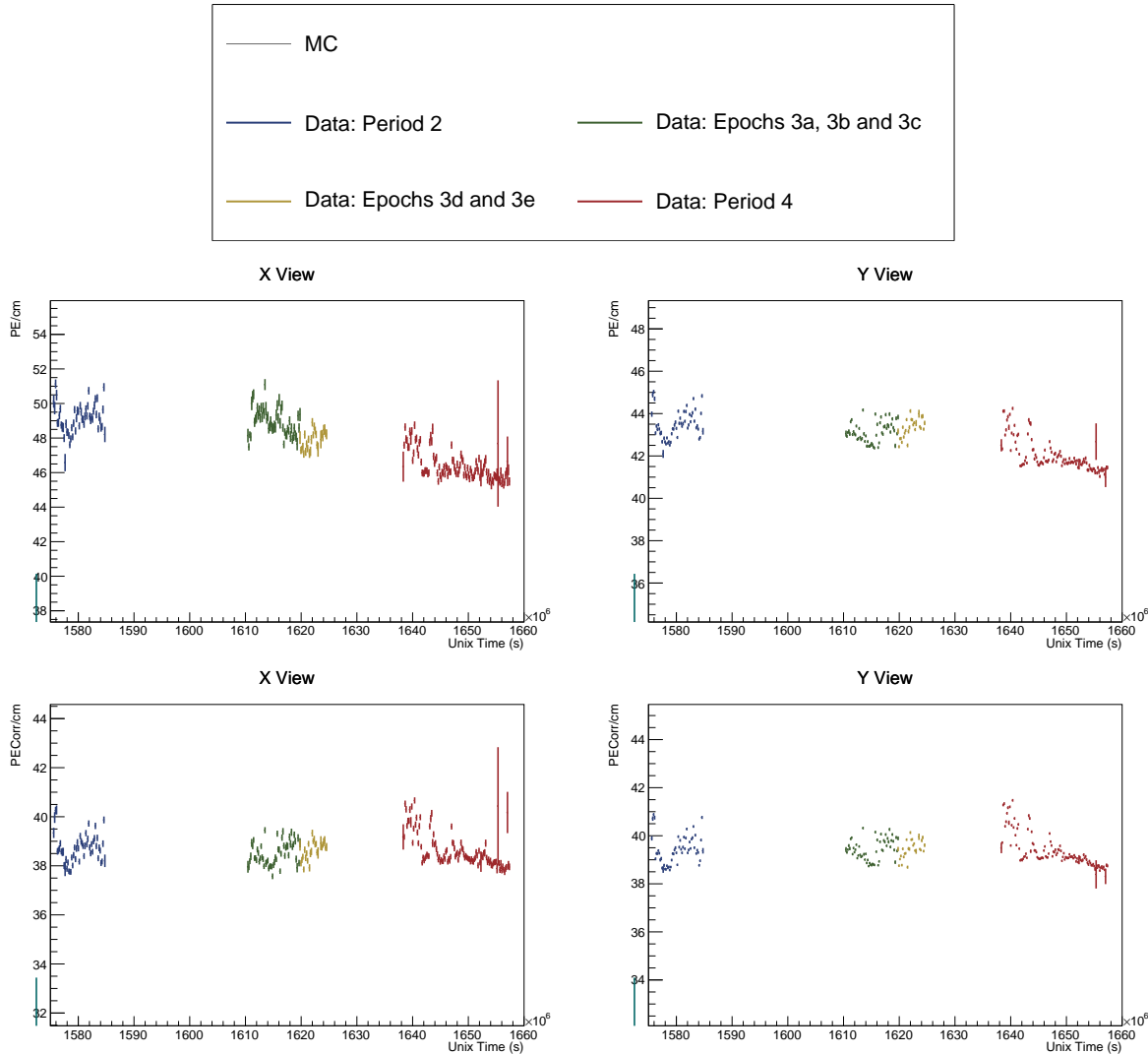


Figure 39: ...

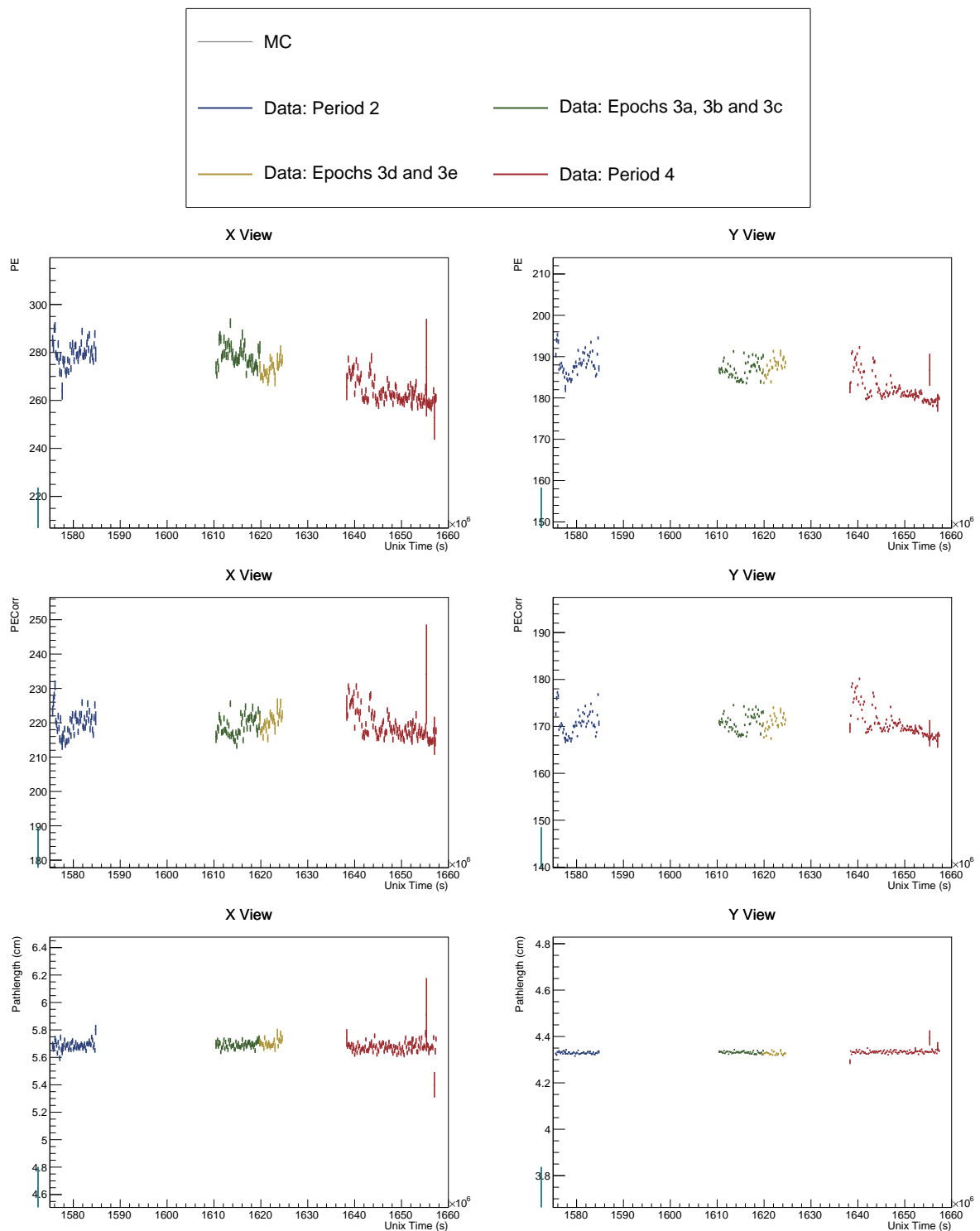


Figure 40: ...